Chapter 3

Synthesis and Study of Curcuminoid based Cryptand as Drug Carrier

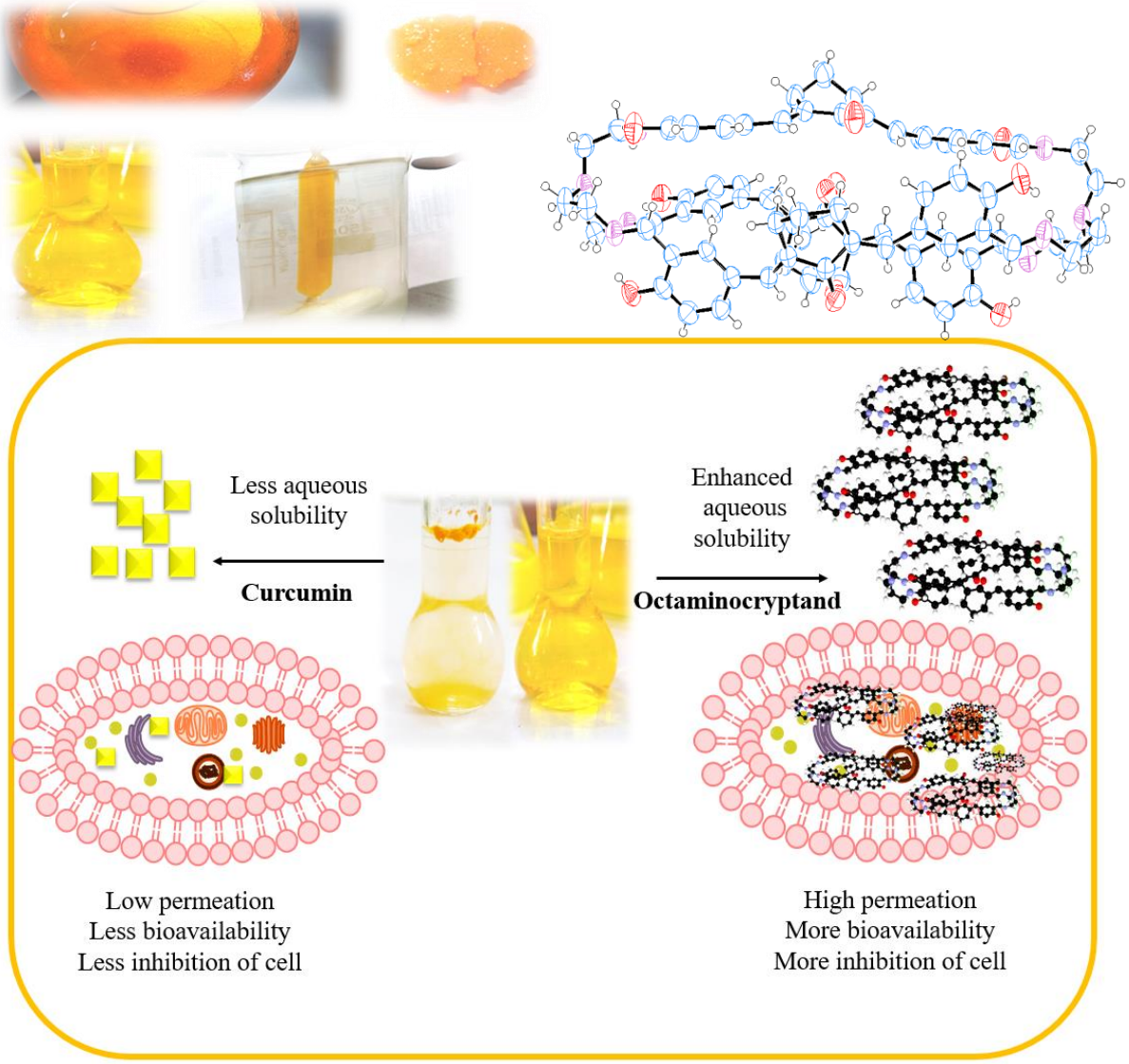

3.1. Introduction

The first diazabicyclic cryptand "katapinand" Park and Simmons in 1968 invented the first. Lehn et al coined the term "cryptand" to describe bicyclic ligands[1-3]. The name "cryptand," comes from the Greek word kruptos, which means "hidden," because the inner or binding cavity of a cryptand is "hidden" from the outward solvation shell and the encapsulated guest will be free from bulk solvent effect[4]. Cryptands are bicyclic or oligocyclic macroheterocycles with greater association constants than crown ethers. As compared to crown ether analogues, cryptands are more expensive but highly selective for specific ions. Because the rigidity of the cage better fits the ionic radii, cryptands typically have a larger stability constant[5]. A larger range of control over both the binding and release of guest molecules is provided by the extra arm in case of cryptand which creates steric constraints on the cavity, which enable higher binding affinities to guests. More significantly, the addition of the extra arms of cryptand may make the cryptand-based host-guest system responsive to more stimuli, which is essential for the development of adaptive or smart materials[6].

A greater degree of control over the binding and release of guest molecules may be achieved by replacing an oxygen atom in the cycle with a nitrogen atom and attachment of suitable substituents to it[7].

Cryptands are used for recognition of cations and anions, binding hydrophilic dye molecules and nanometric light converting devices on binding the Ln^{3+} metal ion. Zhang et. al. developed and produced crown ether-based cryptands in the last ten years as a new kind of host for small organic guests with the aim of greatly enhancing the stabilities of the host-guest complexes and more effectively preparing mechanically interlocked structures and large supramolecular systems while maintaining or improving their stimuli-responsiveness. The creation of useful supramolecular aggregates has frequently utilised organic compounds such as paraquat derivatives and secondary ammonium salts (figure 3.1). A variety of host molecules, such as crown ethers, cyclodextrins, calixarenes, cucurbiturils, pillararenes, and cryptands, have been used to create self-assembled structures with these guest molecules. However, due to their preorganization and additional, optimised binding sites, cryptands show the best stability with paraquat derivatives in organic solvents[8].

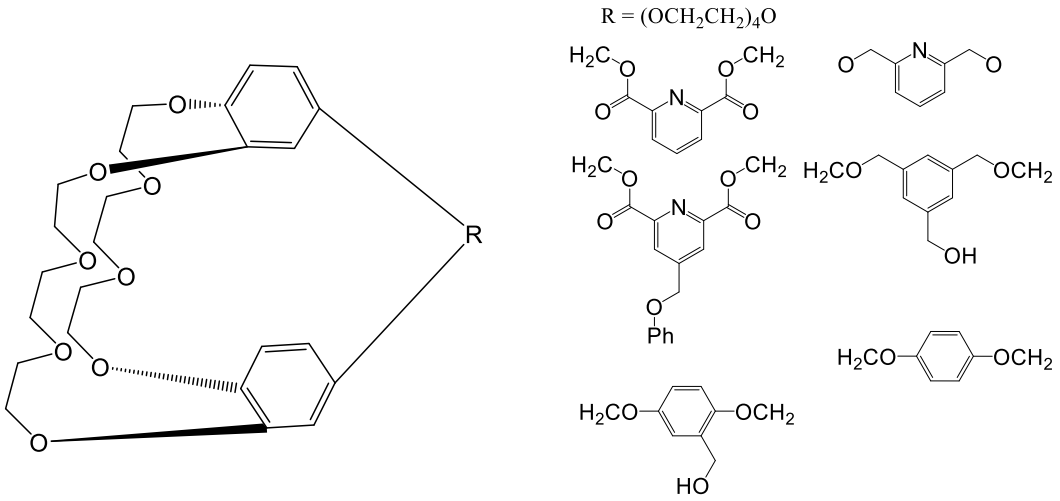

Figure. 3.1. Structure of cryptand synthesized by Zhao et. al.

Recently, McDonagh et. al. reported the synthesis of bi-functional [2.2.2]- cryptands (CRYPT) and the demonstrated radiolabeling of CRYPT with Pb^{2+} isotopes (figure 3.2). They showed that the complexation efficiency of developed system was higher than DOTA (1,4,7,10-tetraazacyclododecane-1,4,7,10-tetraacetic acid) and comparable to the current industry standard TCMC (1,4,7,10-tetraaza-1,4,7,10-tetra-(2- carbamoylmethyl)-cyclododecane),. Additionally, they carry out *in vitro* human blood stability experiments, which showed good [^{203}Pb]Pb-CRYPT stability over a 72-hour period (91.7 0.56%; n = 3). A new industry norms for therapeutic and diagnostic radio-metals in radiopharmaceutical elaboration can be set by discovery of potential of [^{203}Pb]Pb-CRYPT[9].

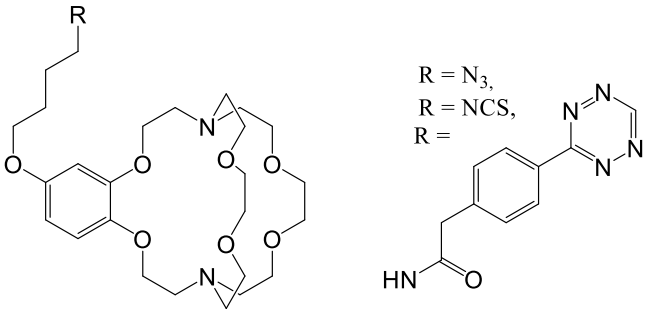

Figure. 3.2. Structure of bifunctional [2.2.2] cryptand synthesized by McDonagh et. al.

There are lots of cryptands which are reported till date[10-35] but the application of cryptand in the field of drug delivery is limited. To study the capabilities of the cryptand as drug carrier we synthesized a novel cryptand based drug carrier from tripodal amine and cyclohexanone based curcuminoid.

3.2. Experimental Section

3.2.1. Materials

The chemicals and solvents used in the preparation of curcuminoid based hexaiminocryptand and octaminocryptand were of analytical grade and purchased from Merck, Spectrochem, Loba chemicals, TCI and SRL. Chemicals were used without further purification.

3.2.2. Synthesis of hexaiminocryptand[36]

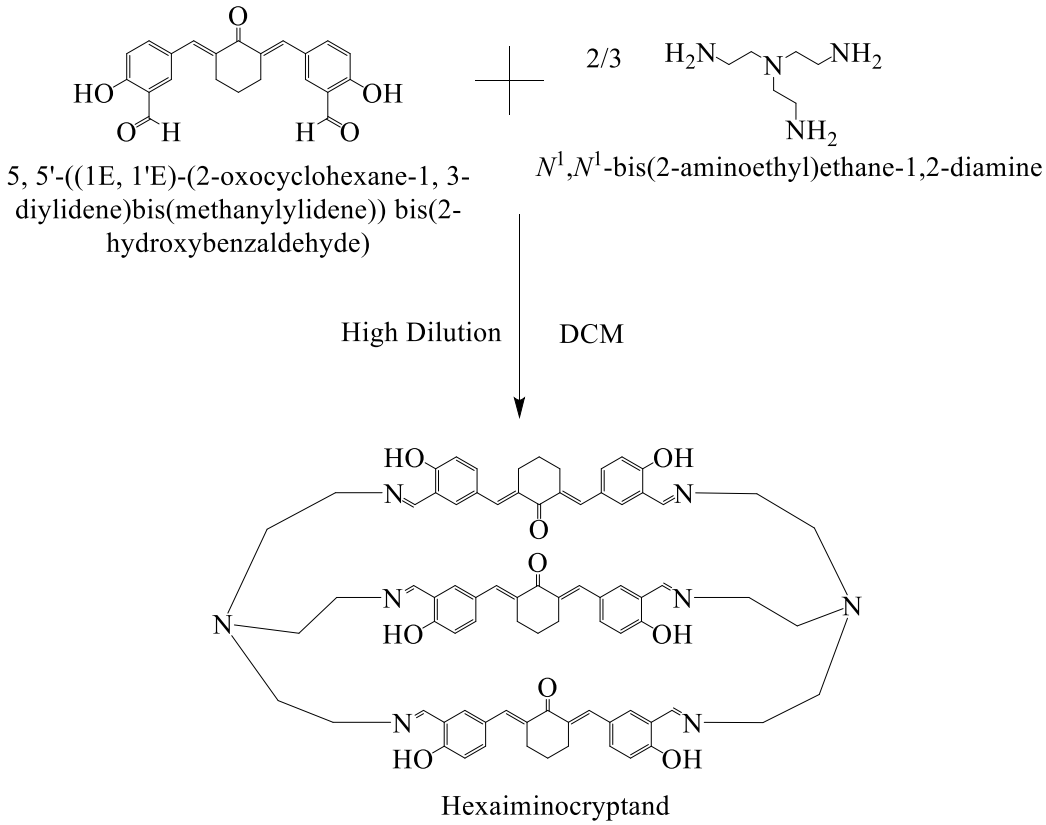

Scheme. 3.1. Synthesis of Hexaiminocryptand.

2 L DCM (Dichloromethane) was placed in a 5 L round bottom flask. 1 g (0.0027 moles) of bis-aldehyde and 0.27 g (0.0018 moles) of TREN (Tris-2-aminoethylamine) were dissolved in 750 ml of DCM individually. Both solutions were added drop wise to mechanically stirred DCM kept in a round bottom flask over 7 to 8 hours. The reaction mixture was concentrated to 100 ml and kept for slow evaporation to obtain intense orange crystalline product.

Yield: 77 %

M. P.: 216 °C (degraded)

FT-IR (KBr disc, cm^{-1}): 3443.67(ν_{-OH}), 2931.40(ν_{-CHas}), 2832.15(ν_{-CHs}), 1635.92($\nu_{-C=N}$), 1594.57($\nu_{-C=C}$).

^{1}HNMR: (400 MHz, $CDCl_3$): δ 14.73 (1H, s), 7.69 (1H, J_1 = 8.8 Hz, J_2 = 2.0 Hz, dd), 7.65 (1H, s), 7.33 (1H, s), 7.09 (1H, J = 8.4, d), 6.31 (1H, J = 1.6, d), 3.54 (2H, d), 2.97 (2H, t), 2.74 (2H, t), 1.69 (1H, quint).

^{13}C NMR: (400 MHz, $CDCl_3$): δ 189.01, 165.57, 162.87, 135.25, 134.92, 134.16, 133.73, 126.77, 118.00, 117.94, 57.83, 57.69, 28.08, 22.64.

DEPT135 NMR: (400 MHz, $CDCl_3$): δ 165.58, 135.29, 134.93, 133.75, 118.04, 57.80, 57.64, 28.09, 22.64.

HRMS: 1293.5773 [M+23] (Theoretical Mass [M+23] = 1293.5892).

3.2.3. Reduction of hexaiminocryptand[36]

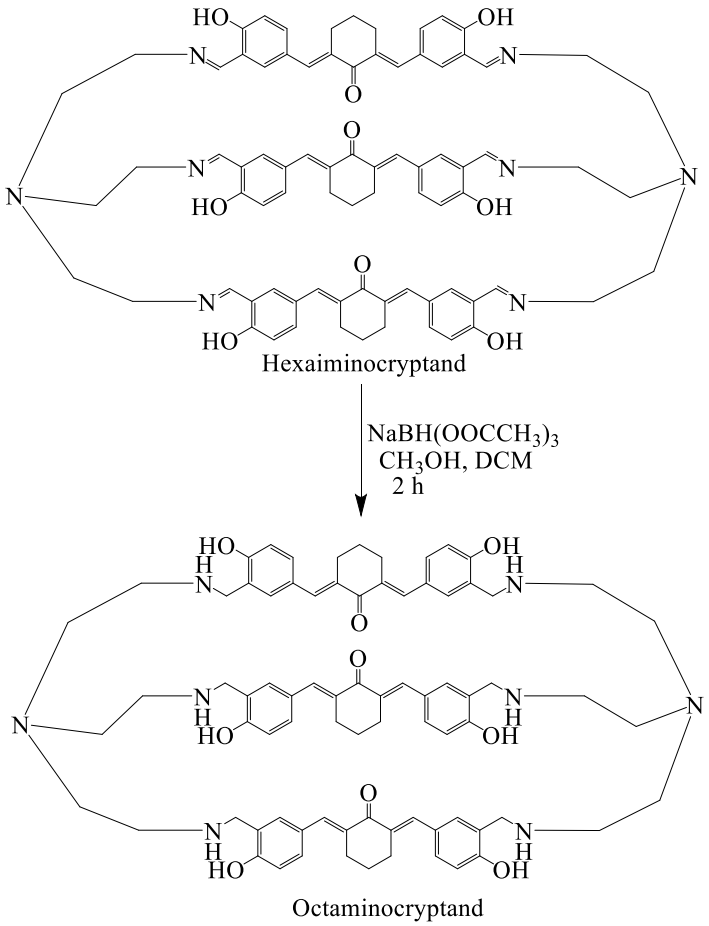

Scheme. 3.2. Reduction of hexaiminocryptand to produce octaminocryptand.

The hexaiminocryptand (1 g, 0.00079 moles) was dissolved in 100 ml DCM (dichloromethane) and 300 ml methanol. Added sodium triacetoxyborohydride (6.0 g, 0.028 moles) to magnetically stirred solution of hexaiminocryptand. The solution was stirred for 5-6 hours. Methanol was evaporated under vacuum completely. Residue was quenched in liquor ammonia and extracted with DCM. The DCM layer was dried over sodium sulphate and evaporated to obtain the desired product. The formed octaminocryptand was dried under high vacuum to obtain red free flowing solid.

Yield: 90 %

M. P.: 211 ºC (degraded)

FT-IR (KBr disc, cm^{-1}): 3387.70(ν_{-OH}), 2926.60(ν_{-CHas}), 2835.12(ν_{-CHs}), 1639.54($\nu_{-C=O}$), 1589.07($\nu_{-C=C}$).

^{1}H NMR: (400 MHz, DMSO-d_6): δ 7.48 (1H, s), 7.15 (1H, *J* = 8.4, d), 7.10 (1H, s), 6.59 (1H, *J* = 8.4, d), 3.78 (2H, s), 2.74 (2H, s), 2.59-2.50 (4H, m) 1.44 (1H, s).

^{13}C NMR: (400 MHz, DMSO-d_6): δ 188.44, 174.93, 136.69, 132.62, 132.28, 131.41, 125.57, 124.17, 116.61, 53.98, 50.78, 46.70, 28.42, 23.00.

DEPT135 NMR: (400 MHz, DMSO-d_6): δ 136.69, 132.34, 131.53, 116.70, 53.78, 50.20, 46.67, 28.42, 23.09.

HRMS: 1281.6627 [M-1] (Theoretical Mass [M-1] =1281.6831).

3.2.4. UV-Vis Study

Drug encapsulation was characterized by UV–Vis spectrophotometry. 4.0 x 10^{-3} M stock solution of drug was prepared in spectroscopy grade DMSO (Dimethyl sulphoxide) solvent. 4 x 10^{-4} M Stock solution of octaminocryptand was also prepared in DMSO. The spectrum of inclusion complex of drug in octaminocryptand was recorded by mixing 2 ml of solution of drug with 2 ml solution of octaminocryptand. Individual spectrum of drug and octaminocryptand were recorded by diluting 2 ml of their solutions with DMSO solvent to make total 4 ml.

3.2.5. NMR titration

The interactions between drug and octaminocryptand were studied by ^{1}H NMR technique. NMR titrations were recorded on 400 MHz Bruker instrument. 0.6 ml 1 x 10^{-2} M solution of standard drugs such as methotrexate (MTX), flutamide (Ft) and gemcitabine hydrochloride

(GEM) were prepared in DMSO-d_6 and placed in NMR tube. NMR titrations were carried out by adding 30 µl, 2 x 10^{-2} M solution of octaminocryptand.

3.2.6. Encapsulation of Methotrexate

Drug Methotrexate (3.5 mg, 0.0077 mmoles)) was dissolved in a solvent N, N'-Dimethylformamide (1 ml). 1 mg (0.00077 mmoles) of octaminocryptand was also dissolved in the same solvent (1 ml) and mixed with the solution of drug. The inclusion complex of drug with octaminocryptand got precipitated out instantly. The precipitates were filtered, washed with the solvent and dried in vacuum.

3.2.7. Cumulative release of MTX

Dialysis bag method[37] was used to investigate the cumulative release profile of MTX at two different pH levels (7.4 and 5.5). Briefly, 1 kD MWCO, S/P 6 trial kit, 18 mm, Dialysis tubing from Repligen (Spectrum Laboratories), Inc. was used for dialysis. 2.0 mg of inclusion complex was used for an experiment. 100 ml of buffer at pH 5.5 and pH 7.4 were used as release medium. A predefined volume of the release medium (5 ml) was withdrawn at regular intervals, and an equal volume of freshly made buffer was then supplied to make up for this withdrawal. Each sample was generated in triplicate, and a UV-visible spectrophotometer was used to determine the concentration of the drug released.

3.2.8. Cytotoxicity assay

The MTT colorimetric assay was performed to evaluate the in vitro cytotoxic activity of octaminocryptand, inclusion complex and MTX against HeLa and MCF-7 cells. Firstly, both cell lines were maintained under appropriate condition environment. HeLa and MCF-7 cells were harvested in minimum essential medium (MEM) supplemented with 10% Fetal Bovine Serum (FBS) and maintained at 37°C supplemented with 100 I. U./ml Penicillin-Streptomycin, 5 % CO_2 in a CO_2 incubator (Remi, India) with 95% humidity. The cell lines obtained from each log-phase of growth were harvested by trypsinization and then resuspended in complete growth medium to give a total of 2×10^4 cells/ml. Then, 200 µl of the cell suspension was seeded into the wells of 96-well plates (Tarson). The plates were incubated overnight in a humidified air atmosphere at 37°C with 5% CO_2. After overnight incubation, the cells were treated with the compounds in concentration range of 0.01-300 µg/ml. The plates were incubated for further 24 h. At the highest concentration of the compounds applied, DMSO accounted for 0.2% of the final concentration. In each plate three control wells (cells without test compounds) and

blank wells (the medium with 0.2% DMSO) were kept for cell viability determination. After completion of 24 h incubation time, 10 µl MTT (5 mg/ml), was added to each wells, followed by 4 h of incubation. After incubation, in each well, the culture medium was then replaced with 100 µl of DMSO. After 30 min incubation the plate was shaken for 1 min and then using a microplate reader (Analabs), the absorbance of each well was measured by at 490 nm. For each compound, the concentration that inhibits 50% cell growth has been determined (IC_{50}).

3.2.9. In vivo study

Male and female Wistar rats (150-250 grams) were procured from Global Bioresearch Solutions Private Limited, Pune CPCSEA approved animal supplier. Animals were maintained under standard laboratory conditions at temperature 22 ± 3ºC with relative humidity 30% - 70% on a 12 h/12 h light/dark cycle. Animals had free access to food (Nutrivet Pvt Ltd, Pune) and water ad libitum. The animals were moved to the experimental area 1h prior to the experiment. All the experiments were performed according to the Committee for the Purpose of Control and Supervision on Experiments on Animals (CPCSEA) and were approved by the Institutional Animal Ethics Committee Bharati Vidyapeeth (Deemed to be University) with approval number PCP/ IAEC/ 2023/ 4-14.

Acute oral toxicity studies (OECD 423) in female Wistar rats were performed for octaminocryptand, inclusion complex, and MTX as per OECD guidelines 423. The Animals will divided into 4 groups of 3 animal each. They will be administered with vehicle, octaminocryptand, inclusion complex, and MTX by oral route at the doses of 300 mg/Kg. The animals will be observed individually for any sign of changes in behaviour and physiological appearance, with special attention during the first 4 h then periodically during the first 24 h. All the animals will be observed for signs of toxicity, morbidity and mortality for 14 days. Observations focused on determining any signs of toxicity, such as changes in skin and fur, eyes and mucous membranes, and also respiratory, circulatory, autonomic and central nervous systems, and somatomotor activity and behaviour pattern. Attention should be directed to observations of tremors, convulsions, salivation, diarrhoea, lethargy.

3.2.10. Encapsulation of Flutamide (Ft)

Flutamide 10.7 mg, 0.0387 mmoles was kneaded in mixture of solvent of methanol and water (2 ml) with 5 mg, 0.0038 mmoles of octaminocryptand. The resultant mixture were then

sonicated and kneaded in dark condition. It was allowed to dry for few days. Free flowing powder was obtained.

3.2.11. Calculation of Drug Loading (DL%) of Octaminocryptand and Encapsulation Efficiency (EE%) of Flutamide

2 ml aqueous solution of the 6.5 mg of inclusion complex was dialysed using a dialysis bag (MWCO: 1 kD) in 100 ml of aqueous medium at 37 °C to calculate the drug loading and encapsulation efficiency. Utilising an ultraviolet detection wavelength of 287 nm, a UV-Vis spectrophotometry was used to quantify the amount of medication contained in the inclusion complexes. Using the following formulae[38], the drug loading (DL) and entrapment efficiency (EE) were estimated in comparison to the standard curve:

$$DL\ (\%) = [(W_{Flutamide} - W_{Unbound\ Flutamide}) / W_{Inclusion\ complex})] \times 100$$

$$EE\ (\%) = [(W_{Flutamide} - W_{Unbound\ Flutamide}) / W_{Flutamide})] \times 100$$

Where,

$W_{Flutamide}$ = Weight of flutamide in inclusion complex

$W_{Unbound\ Flutamide}$ = Weight of unbound flutamide released from inclusion complex

$W_{Inclusion\ complex}$ = Weight of inclusion complex

3.2.12. Cumulative release of Flutamide

2 ml of the 2.7 mg of inclusion complex in aqueous solution was dialysed using a dialysis bag (MWCO: 1 kD) in 100 ml of the buffer solution at 37 °C. The study was carried out with PBS (Phosphate buffer solution) of pH 5.5. PBS with pH 5.5 simulates the tumour microenvironment. To determine the cumulative drug release, the UV-Vis spectrometer was used to quantify the dialysate at 287 nm during the drug release. A predefined volume of the release medium (5 ml) was withdrawn at regular intervals, and an equal volume of freshly made buffer was then supplied to make up for this withdrawal. Each sample was generated in triplicate, and a UV-visible spectrophotometer was used to determine the concentration of the drug released.

3.2.13. Encapsulation of Gemcitabine hydrochloride

Drug gemcitabine hydrochloride (11.6 mg) was kneaded in mixture of solvent methanol and water (2 ml) with 5 mg of octaminocryptand. The resultant mixture were then sonicated and kneaded in dark condition. It was allowed to dry for few days. Free flowing powder was obtained.

3.2.14. Calculation of Drug Loading (DL %) of Octaminocryptand and Encapsulation Efficiency (EE%) of Gemcitabine hydrochloride

2 ml of the 24.4 mg of inclusion complex in aqueous solution was dialysed using a dialysis bag (MWCO: 1 kD) in 100 ml of aqueous medium at 37 °C to calculate the drug loading and encapsulation efficiency. Utilising an ultraviolet detection wavelength of 266 nm, UV-Vis spectrophotometry was used to quantify the amount of drug contained in the inclusion complexes. Using the following formulae, the drug loading (DL) and entrapment efficiency (EE) were estimated in comparison to the standard curve:

$$DL\ (\%) = [(W_{\text{Gemcitabine hydrochloride}} - W_{\text{Unbound Gemcitabine hydrochloride}}) / W_{\text{Inclusion complex}})] \times 100$$

$$EE\ (\%) = [(W_{\text{Gemcitabine hydrochloride}} - W_{\text{Unbound Gemcitabine hydrochloride}}) / W_{\text{Gemcitabine hydrochloride}})] \times 100$$

Where,

$W_{\text{Gemcitabine hydrochloride}}$ = Weight of gemcitabine hydrochloride in inclusion complex

$W_{\text{Unbound Gemcitabine hydrochloride}}$ = Weight of unbound gemcitabine hydrochloride released from inclusion complex

$W_{\text{Inclusion complex}}$ = Weight of inclusion complex

3.2.15. Cumulative release of Gemcitabine hydrochloride

2 ml of the 12.1 mg of inclusion complex in aqueous solution was dialysed using a dialysis bag (MWCO: 1kD) in 100 ml of the buffer solution at 37 °C. The study was carried out with PBS (Phosphate buffer solution) of pH 7.4 and PBS of pH 5.5. PBS of pH 7.4 mimics the normal physiological medium and PBS with pH 5.5 simulates the tumour microenvironment. To determine the cumulative drug release, the UV-Vis spectrometer was used to quantify the dialysate at 266 nm during the drug release. Each sample was generated in triplicate, and a UV-visible spectrophotometer was used to determine the concentration of the drug released.

3.2.16. Cell line and culture condition

The MDA-MB-231 were procured from the National Centre of Cell Sciences, Pune and cultured in Leibovitz-15 (L-15) medium supplemented with 10% v/v heat-inactive foetal bovine serum (FBS) (HiMedia), 100 I.U./ml penicillin-streptomycin solution at 37°C and in a humidified atmosphere of 5% CO_2 in the air. The cell viability of the cells was measured with the staining of the cells with 0.25% trypan blue dye and counted in a haemocytometer under an inverted microscope.

3.2.17. Cell Cytotoxicity Assay

In 96-well plates (1×10^5 cells/ml) were seeded (100 µl/well) and incubated for 24 hours (cell recovery and attachment). The synthesized complexes, and the negative control substance dimethyl sulfoxide (DMSO) 0.2% were added to the healthy plates and again incubated for 24 hours. The healthy plates were then incubated with 10 µl of 3-(4,5-Dimethylthiazol-2-yl)-2,5-Diphenyltetrazolium Bromide (MTT) (5 mg/ml stock). MTT was removed after the 4-hour incubation period, and 100 µl of DMSO was added to dissolve the formazan crystals. The concentration was measured at 490 nm in a microplate reader, and the findings were displayed as a percentage inhibition (50% inhibition).

3.2.18. Characterization Method

FT-IR studies of all compounds were performed on Bruker Alpha FT-IR spectrometer in solid state as KBr pellets. UV-visible Spectrophotometer experiments were performed on Perkin Elmer Lambda 35 Spectrophotometer, Inc, MA, USA. NMR data was recorded on Bruker AVANCE, 400 MHz spectrometer in $CDCl_3$ and DMSO-d_6, with TMS as internal standard. An Xcalibur, EOS, Gemini diffractometer was used to acquire diffraction data for all of the synthesized compounds using graphite monochromatic Mo Kα radiation (0.71073). The Olex 2 software and the ShelXL refinement package were used to solve and refine all structures. MERCURY was used to create the graphics (version 3.9). Direct approaches were used to solve all structures, which were then refined in a regular way. Non-hydrogen atoms were treated anisotropically in all circumstances. The thermogram were investigated by differential scanning calorimeter (DSC) using a Perkin Elmer Thermal Analyzer with heating and cooling rate 10 °C min^{-1}.

3.3. Result and discussion

In this work, in order to develop hexaiminocryptand molecule, we used bis-aldehyde[39,40] synthesized in second chapter and TREN (Tris-2-aminoethylamine). The cyclocondensation reaction via high dilution method in dichloromethane between bis-aldehyde and tetramine produced the [3+2] cyclocondensed hexaiminocryptand (scheme 3.1) (figure 3.3). The pure crystalline product was obtained in 77 % yield which is further characterized by FT-IR, NMR, SC-XRD and HRMS.

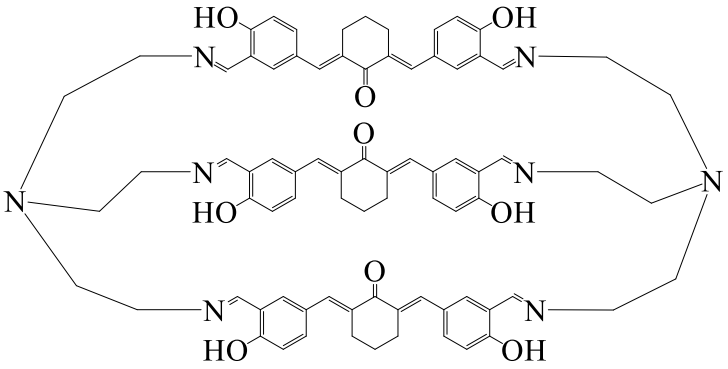

Figure. 3.3. Structure of Hexaiminiocryptand.

In the FT-IR spectrum, the phenolic –OH group of parent bis-aldeyde appeared at 3214.61 cm^{-1} (chapter 2, spectrum 2.3) which is shifted to 3443.67 cm^{-1} (spectrum 3.1) after the formation of hexaiminocryptand, while a new stretching band of imine functionality appears at 1635.92 cm^{-1} (spectrum 3.1). The asymmetric stretching of $–CH_2$ is observed at 2931.40 cm^{-1} and symmetric stretching is observed at 2832.15 cm^{-1}. The asymmetrical alkene group showed stretching at 1594.57 cm^{-1} due to the extended conjugation.

A symmetrical cryptand structure was evident in the ^1H NMR spectrum (spectrum 3.2). A new peak of imine proton is generated at 7.65 ppm and the peak of aldehydic proton at 9.96 ppm (chapter 2, spectrum 2.4) is vanished. The proton of the phenolic hydroxyl group moved downfield to 14.73 ppm due to hydrogen bonding interaction with imine moiety. In aromatic region a double doublet is observed at 7.69 ppm with coupling constant 8.8 Hz and 2.0 Hz corresponds to an aromatic proton para to imino group indicating ortho and meta coupling respectively. A doublet at 7.09 ppm with coupling constant 8.4 Hz corresponds to aromatic proton meta to imine group and a doublet at 6.31 ppm corresponds to aromatic proton ortho to

imino group. A singlet of a vinylic proton attached to the carbon containing aromatic ring is observed at 7.33 ppm. A doublet at 3.54 ppm corresponds to methylene proton attached to imine moiety while a triplet at 2.97 ppm corresponds to the methylene proton attached to tertiary nitrogen. The methylene protons of cyclohexanone moiety appear as a triplet at 2.74 ppm and as a quintet at 1.69 ppm.

The symmetrical structure of hexaiminocryptand is represented by the 14-peak in ^{13}C NMR (spectrum 3.3) and 9 peaks in DEPT135 spectrum (spectrum 3.4). The DEPT135 spectrum of hexaiminocryptand showed 4 negative peaks due to methylene carbon and 5 positive peaks due to methine carbon.

The [3+2] cyclocondensation was confirmed by the HRMS (spectrum 3.5), [M+23] peak is observed at 1293.5773 m/z which is in good accordance with the calculated value 1293.5892 m/z.

The structure of hexaiminocryptand was confirmed by the SC-XRD analysis. The crystals were developed from dichloromethane by slow evaporation method. The structure analysis showed that three moiety of bis-aldehyde is joined with two moieties of TREN(Tris-2-aminoethylamine) via an imine linkage and thus produced capsule like cavity with the dimension of 19.822 Å x 7.569 Å x 4.498 Å (figure 3.4).

A.

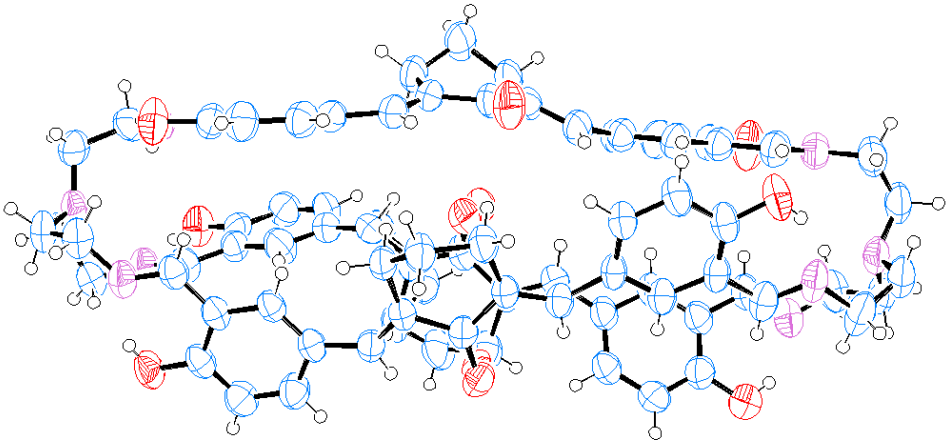

B.

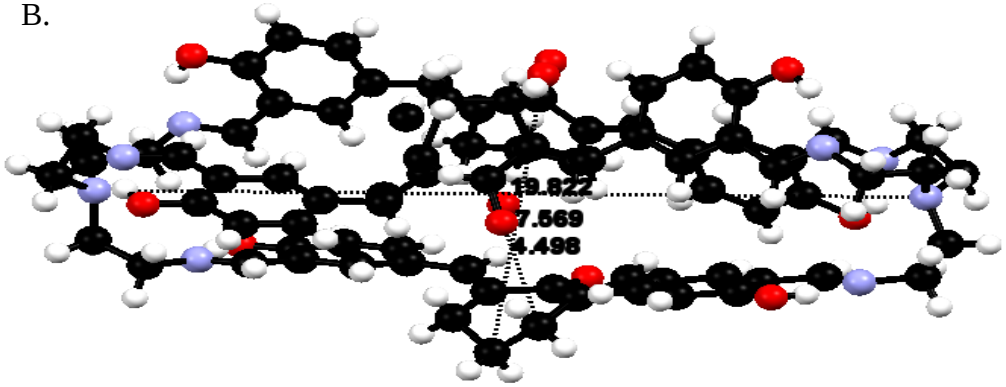

Figure. 3.4. A.) ORTEP diagram of hexaiminocryptand, B.) Intrinsic cavity dimension of hexaiminocryptand.

Empirical formula	$C_{78}\ H_{78}\ N_8\ O_9$
Temperature (K)	293
Crystal system	monoclinic
Space group	$P2_1/c$
a (Å)	19.4906(6)
b (Å)	14.7448(5)
c (Å)	23.9937(10)
α (°)	90
β (°)	101.765(4)
γ (°)	90
Volume ($Å^3$)	6750.57
Z	4

Table. 3.1. Crystal data of hexaiminocryptand.

The hexaiminocryptand crystallises in monoclinic crystal system with $P2_1/c$ space group and the asymmetric unit contains one unit of macrocycle (table 3.1). The earlier synthesized tetraiminochiralcorand in chapter 2 with the same bis-aldehyde group showed that the plane of both aromatic ring and cyclohexanone ring were same but in the formation of hexaiminocryptand, three bis-aldehyde moieties got incorporated in such a way that, out of three, two showed the similar orientation as seen in tetraiminochiralcorand but the third moiety of bis-aldehyde showed that both aromatic rings were distorted from their plane and the torsion angle between both the plane is 55.87 ° (figure 3.5).

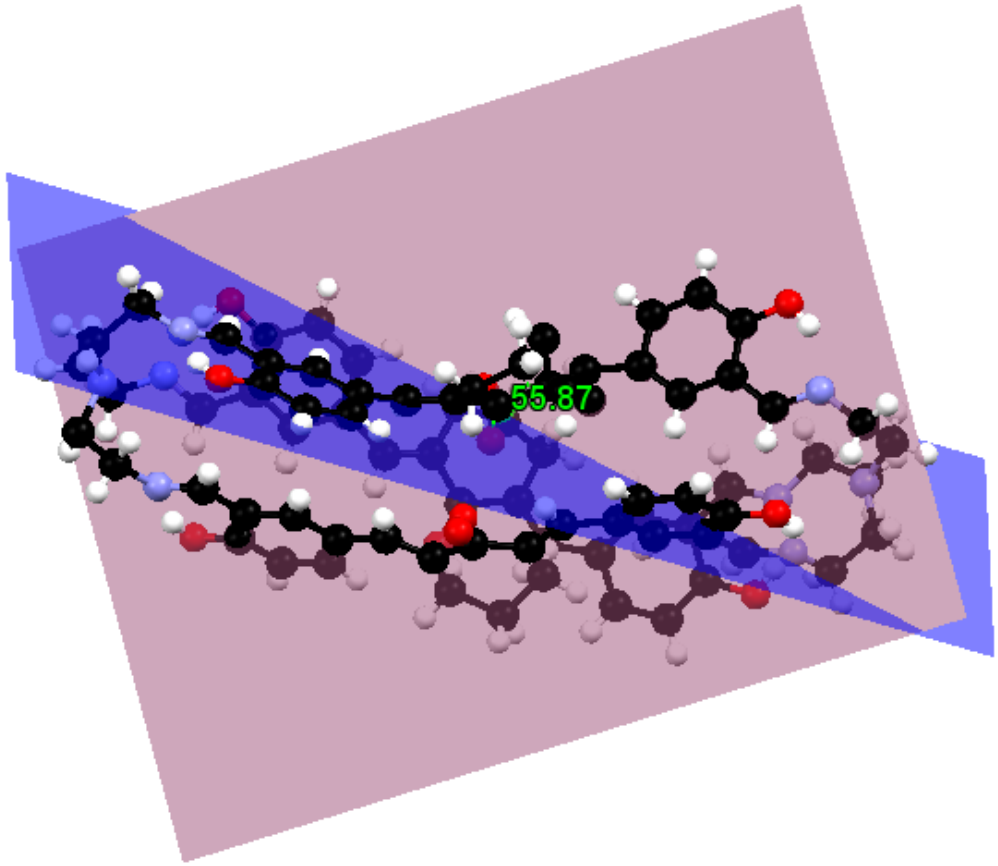

Figure. 3.5. Torsion angle between both the aromatic rings of same arm of hexaiminocryptand.

This might be related to the orientation of half chair form of cyclohexanone. In two of the curcuminoid moiety, the cyclohexanone ring showed half chair form from its fourth number of carbon while the third curucminoid moiety showed the half chair form from third number of carbon. This change in the position of half chair might be possible due to the formation of CH----π interaction in between the hydrogen of the third number of carbon with the alkene group

of curcuminoid moiety of other arm. Due to the strong vibration of atoms, this carbon splitted and showed the van der waals interaction with the oxygen of hydroxyl group of another cryptand molecule. These both non-covalent interaction can explain the half chair form of third curcuminoid moiety from the third carbon of cyclohexanone (figure 3.6). The distance of both the group from distorted -CH were 2.777 Å and 2.547 Å. This distortion further expanded to the aromatic ring, hence the aromatic ring distorted from its plane about 55.87 °.

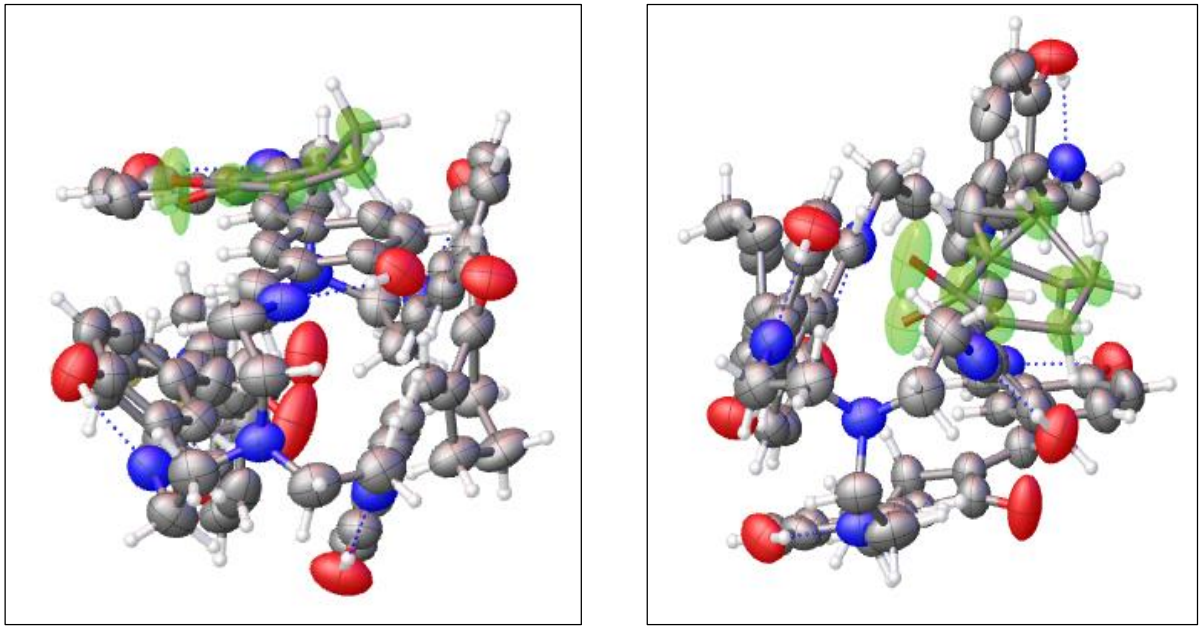

Figure. 3.6. Half-chair conformation of cyclohexanone moiety of hexaiminocryptand A.) Half chair conformation from fourth position with respect to carbonyl group of cyclohexanone, B.) Half chair conformation from third position with respect to carbonyl group of cyclohexanone.

Six hydrogen bonds were formed from the nitrogen of imine moiety with the hydrogen of hydroxyl group. Together they created a hydrophilic cavities on the edges and hydrophobic cavities on the centre of this capsule like cryptand molecule. The functional groups of hexaiminocryptand such as imine, hydroxyl and ketone group are oriented on the periphery while aromatic ring creates a hydrophobic interior.

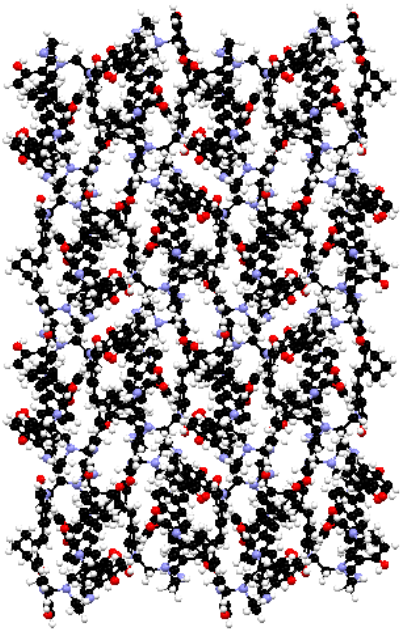

Figure. 3.7. Packing of hexaiminocryptand along ‘a’ axis.

The packing pattern of hexaiminocryptand molecule followed the pattern edge to face due to the presence of non-covalent interaction which creates the extensive void in between the molecule. The packing pattern of cryptand molecule is similar to bee hive (figure 3.7).

The selective reduction by using sodium triacetoxyborohydride of imine bonds of hexaiminocryptand into octaminocryptand introduces the flexibility to the system (scheme 3.2) (figure 3.8).

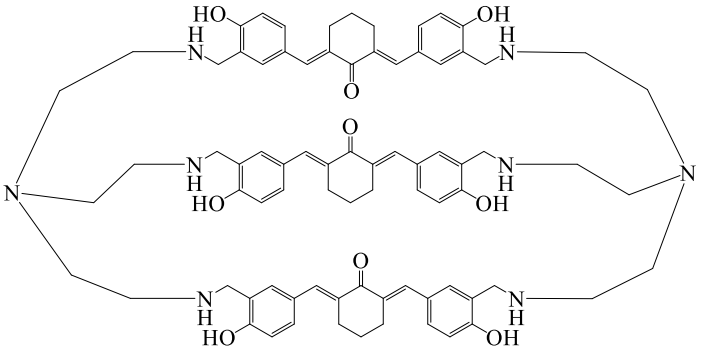

Figure. 3.8. Structure of Octaminocryptand.

The characterization from FT-IR spectrum showed the disappearance of C=N stretching and appearance of –NH stretching at 3387.70 cm^{-1} (spectrum 3.6) which merges with the stretching frequency of –OH group of octaminocryptand. The reduction of imine bonds was also

confirmed by NMR technique. In the ^{1}H NMR spectrum of octaminocryptand (spectrum 3.7) the peak of imine proton vanishes from 7.65 ppm (spectrum 3.2) and the peak due to methylene protons of reduced imine appears as a singlet at 3.78 ppm. The reduction of hexaiminocryptand is also represented by the 15-peak and the positive peak of imine carbon around 165.58 ppm in DEPT 135 spectrum of hexaiminocryptand (spectrum 3.4) is vanished in DEPT 135 spectrum of octaminocryptand (spectrum 3.9) due to reduction of imine bond and a new negative peak at 46.67 ppm is emerged. HRMS showed (spectrum 3.10) [M-1] peak at 1281.6627 m/z which confirms the complete reduction of hexaiminocryptand.

The selective reduction of imine bond of hexaiminocryptand gives the flexibility and aqueous solubility to the system. This property of octaminocryptand helps to deliver the BCS class II and III drug which have low aqueous solubility and low permeability[41]. We chose two drugs from the class of BCS II and one drug from BCS class III drug.

BCS class II drug

A. Methotrexate (MTX)

We chose the drug methotrexate (MTX) for the drug delivery. The inclusion complex of MTX and octaminocryptand was formed by co-precipitation method in N, N'-dimethylformamide. The inclusion complex was characterized by techniques such as FT-IR, UV-Vis, TGA, DSC and NMR. There is change in stretching frequencies of MTX after getting encapsulated in the cryptand (spectrum 3.11 and 3.12). Similarly a bathochromic and hyperchromic shifts are observed in the UV-Vis absorption spectrum of octaminocrypatnd molecule after encapsulation of MTX. The absorption band shifted from 370 nm to 380 nm (figure 3.9).

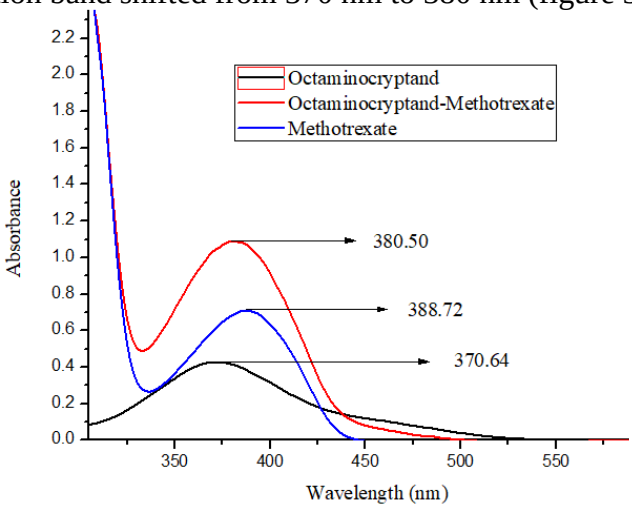

Figure. 3.9. UV-Vis absorption spectra of octaminocryptand, inclusion complex and methotrexate.

This shifting of absorption peak was associated to the non-covalent interactions arise between octaminocryptand and MTX during the encapsulation. These non-covalent interactions change the properties of their parent molecule which clearly reflected in its DSC thermogram (figure 3.10). In the DSC thermogram MTX showed an endothermic peak around 113 °C while octaminocryptand showed two endothermic peak at 108 °C and 162 °C. The physical mixture of cryptand with MTX showed an endothermic peak at 101 °C while the binding of MTX with the cryptand via co-precipitation method form an inclusion complex which showed an endothermic peak at 68 °C.

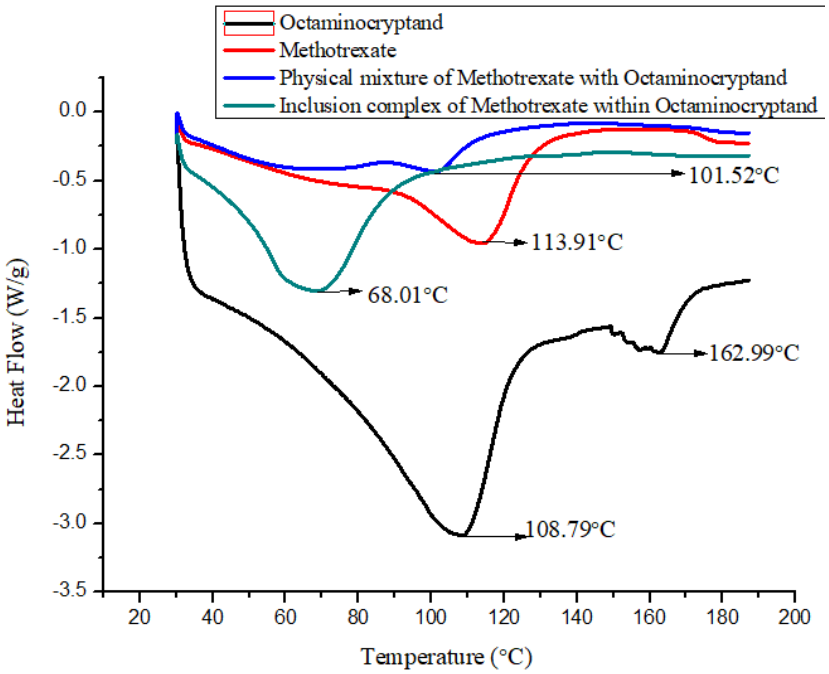

Figure. 3.10. DSC thermogram of octaminocryptand, methotrexate, physical mixture of methotrexate with octaminocryptand and inclusion complex.

We studied the drug binding modes of octaminocryptand by NMR technique. The protons of MTX gives six signals in aromatic region and six in aliphatic region (spectrum 3.13). The amide proton of MTX appears at 8.194 ppm, aromatic proton of pteridine ring appears at 8.580 ppm, aromatic proton ortho to amide group appears at 7.730 ppm and the aromatic proton meta to amide group appears at 6.826 ppm. The proton of $–NH_2$ group of pteridine ring appears at 7.643 and 6.700 ppm. The aliphatic proton of amino methyl group neighbouring to pteridine ring appears at 4.791 ppm. The aliphatic chiral proton neighbouring carboxylic acid and amide group appears at 4.341 ppm. The methyl group of tertiary amine group appears at 3.330 ppm.

The methyl proton neighbouring to carboxylic acid appears at 2.051 ppm and a multiplet 1.941-1.882 ppm of methylene.

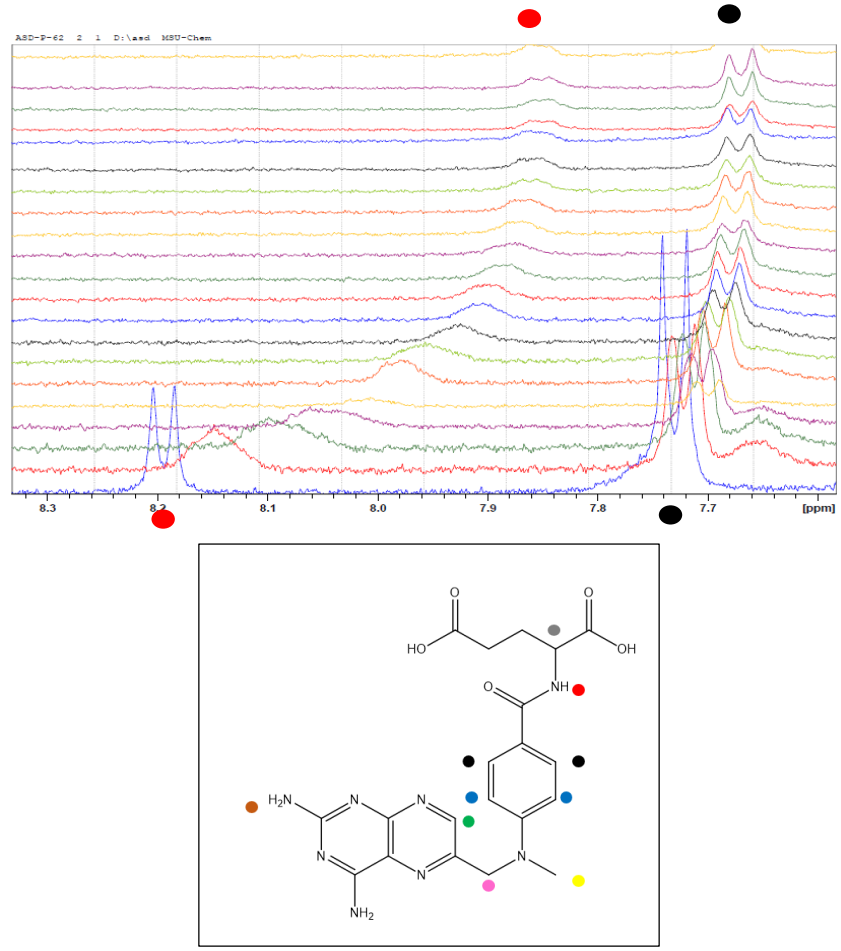

Figure. 3.11. Proton of amide group and proton ortho to the amide group of MTX showed shifting in ^{1}H NMR titration with octaminocryptand.

The ^{1}H NMR titration showed the major chemical shifting of proton of MTX. The active site for binding of MTX with the octaminocryptand are two carboxylic acid groups and the amide group, neighbouring to one of the carboxylic acid group of MTX. The ^{1}H NMR titration revealed the major chemical shifting in the signal of a proton of the amide group of MTX. It is shifted from 8.194 ppm to 7.862 ppm (figure 3.11) and the chiral proton attached to one of the carboxylic acid group of MTX is shifted from 4.341 ppm to 4.226 ppm (figure 3.12). The interaction of these groups with cryptand molecule also affects the environment of aromatic ring attached to amide group of MTX.

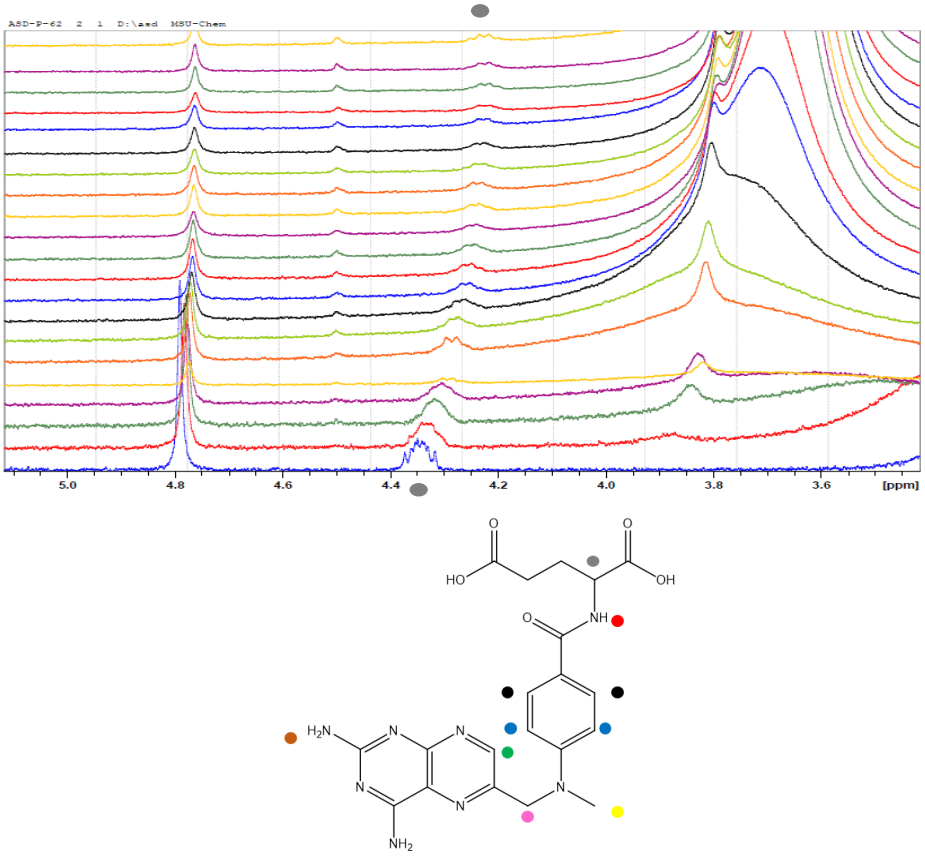

Figure. 3.12. Chiral proton attached to one of the carboxylic acid group of MTX showed shifting in ^{1}H NMR titration with octaminocryptand.

The proton ortho to the amide group showed appreciable chemical shifting from 7.730 ppm to 7.671 ppm (figure 3.11) as compared to proton meta to amide group of MTX which shifts from 6.826 ppm to 6.818 ppm (figure 3.13). This study suggested that the binding between MTX and cryptand are spontaneous.

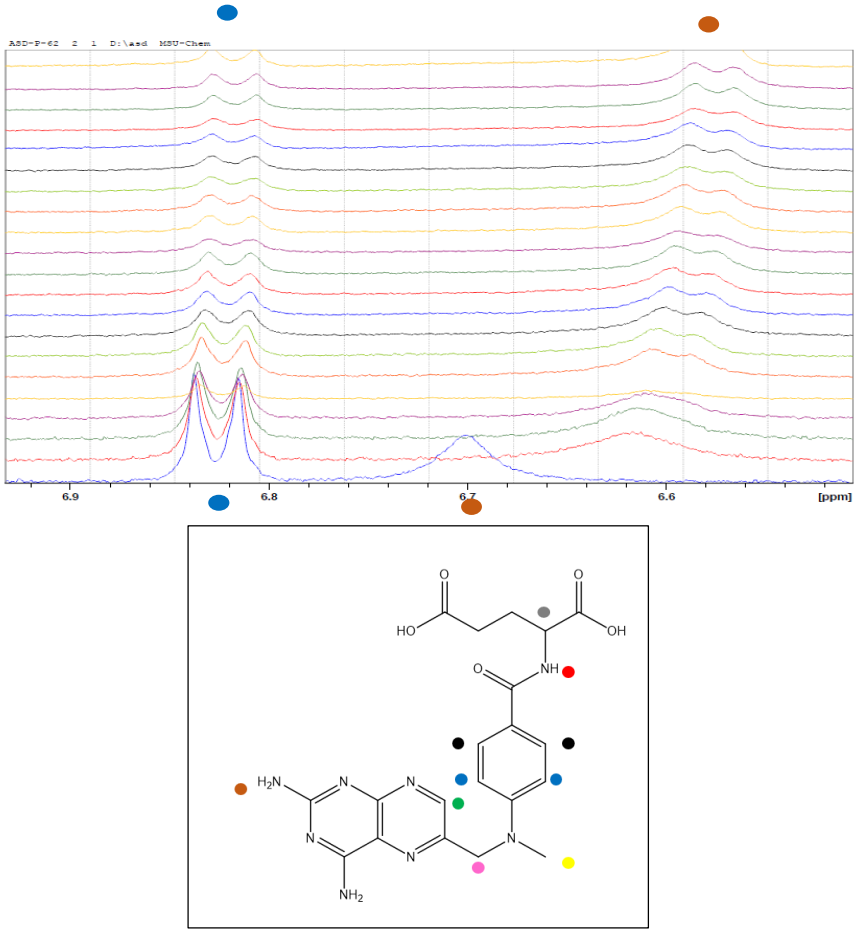

Figure. 3.13. Proton meta to amide group of MTX showed shifting in ^{1}H NMR titration with octaminocryptand.

For better understanding we performed the reverse ^{1}H NMR titration by adding solution of methotrexate to the solution of octaminocryptand in similar manner. The chemical shifting of methylene proton of octaminocryptand attached to nitrogen of secondary amine group and an aromatic ring from 3.754 ppm to 3.768 ppm (figure 3.14), is due to its close vicinity with the amine group of octaminocryptand which might be interacting with carboxylic group of MTX.

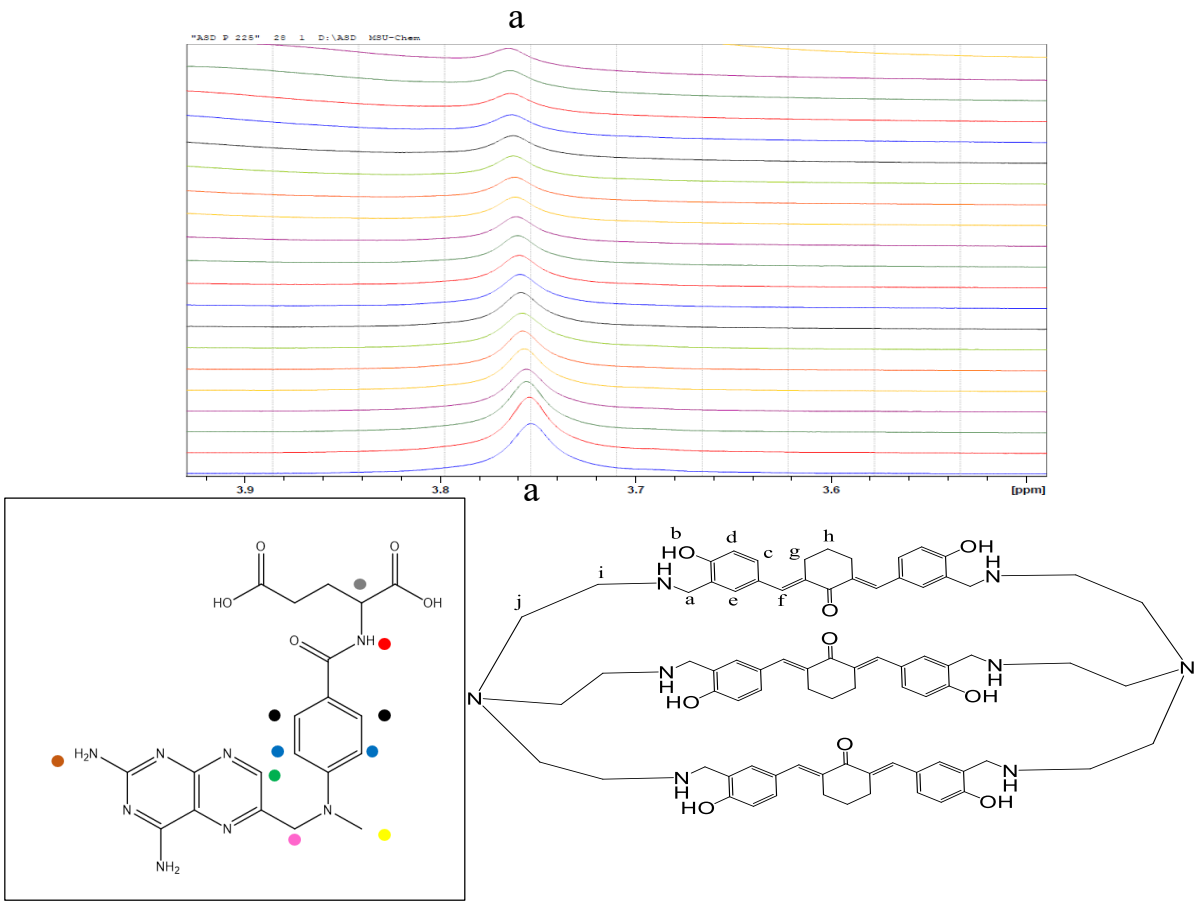

Figure. 3.14. Methylene proton of octaminocryptand attached to nitrogen of secondary amine group showed shifting in ^{1}H NMR titration with MTX (reverse titration).

Through space correlation between the protons of methotrexate and an octaminocryptand molecule in their inclusion complex is investigated by recording the NOESY of inclusion complex of MTX loaded octaminocryptand. There are several cross peaks of proton of octaminocryptand with the protons of MTX observed in the 2DNOESY spectrum of their inclusion complex.

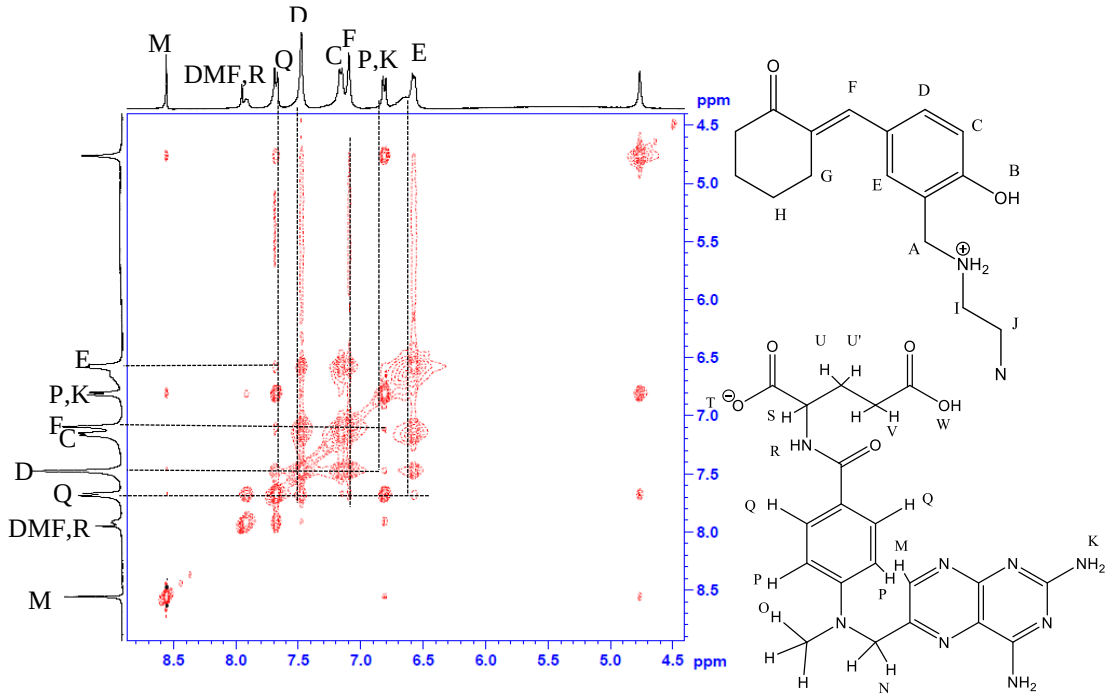

Figure. 3.15. 2D NOESY spectrum of inclusion complex of MTX with octaminocryptand (expansion of downfield region).

The aromatic proton ortho to amide group of MTX in inclusion complex with octaminocryptand appear at 7.679 ppm (spectrum 3.14) showed cross peak with the three proton of octaminocryptand in NOESY (figure 3.15), two are the aromatic proton meta to –OH group of octaminocryptand at 7.477 ppm, 6.576 ppm and one with vinylic proton at 7.095 ppm, revealed the close vicinity between them. The cross peak of aromatic proton (6.811 ppm) meta to amide group of MTX with two proton of octaminocryptand, (the aromatic proton meta to –OH group of octaminocryptand at 7.477 ppm and vinylic proton of octaminocryptand at 7.095 ppm) revealed presence of π-π stacking between them.

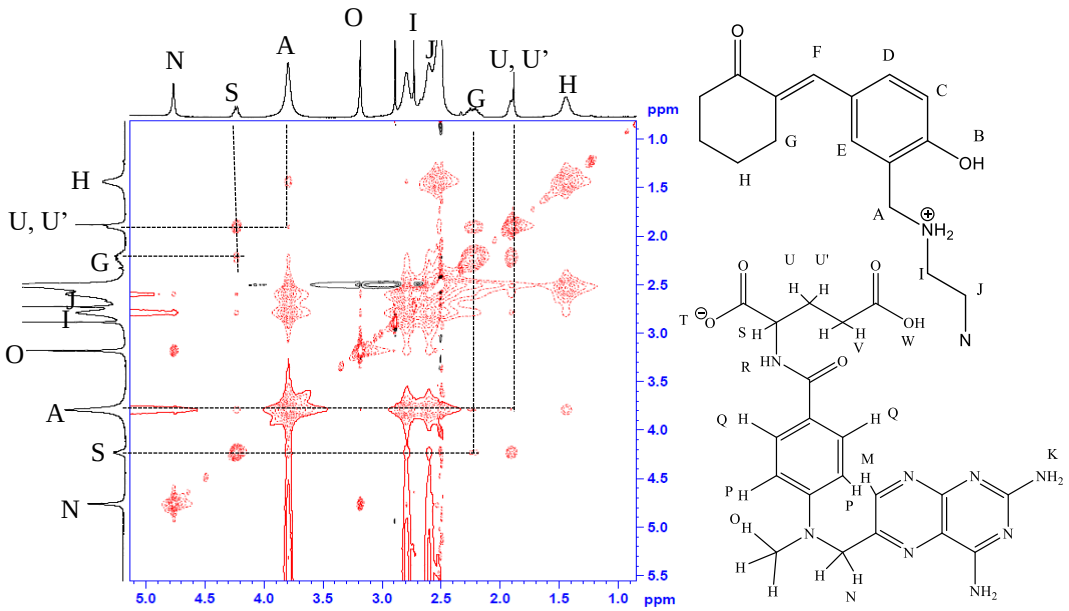

Figure. 3.16. 2D NOESY spectrum of inclusion complex of MTX with octaminocryptand (expansion of upfield region).

Similarly, in aliphatic region of inclusion complex the first cross peak was observed between the aliphatic proton of chiral proton neighbouring to amide and carboxylic acid group of MTX at 4.234 ppm and aliphatic proton of cyclohexanone moiety of octaminocryptand at 2.236 ppm (figure 3.16) while the second cross peak was observed between aliphatic proton of methylene group neighbouring to carboxylic acid group of MTX at 1.885 ppm and the aliphatic proton neighbouring to secondary amine & aromatic ring of octaminocryptand at 3.795 ppm. This reveals the close vicinity of carboxylic group of MTX and amine group of octaminocryptand in their inclusion complex.

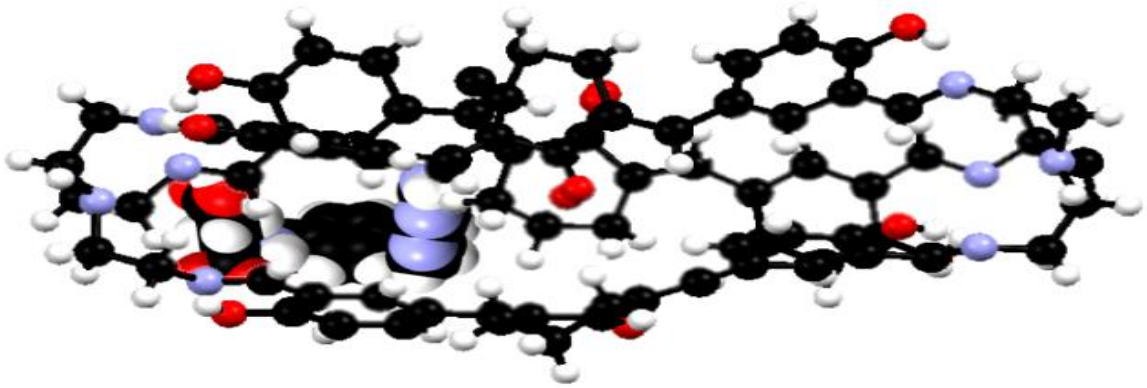

Figure. 3.17. Proposed binding model of Methotrexate with Octaaminocryptand.

On behalf of this study we proposed the mode of binding of MTX with octaminocryptand (image from single crystal structure of hexaiminocryptand is used in lieu of octaminocryptand as model to depict the binding modes figure 3.17). According to the crystal structure of MTX[42], the pteridine ring and carboxylic group is perpendicular to benzamide group which gave it "C" type of orientation. When MTX is encapsulated with octaminocryptand, it might be oriented in such a way that carboxylic group remain present in close vicinity to amine group of octaminocryptand to generate ion-ion interaction while the benzamide ring form π-π stacking with the aromatic ring of octaminocryptand and the amine group of pteridine ring might be forming H-bonding with the oxygen of cyclohexanone ring.

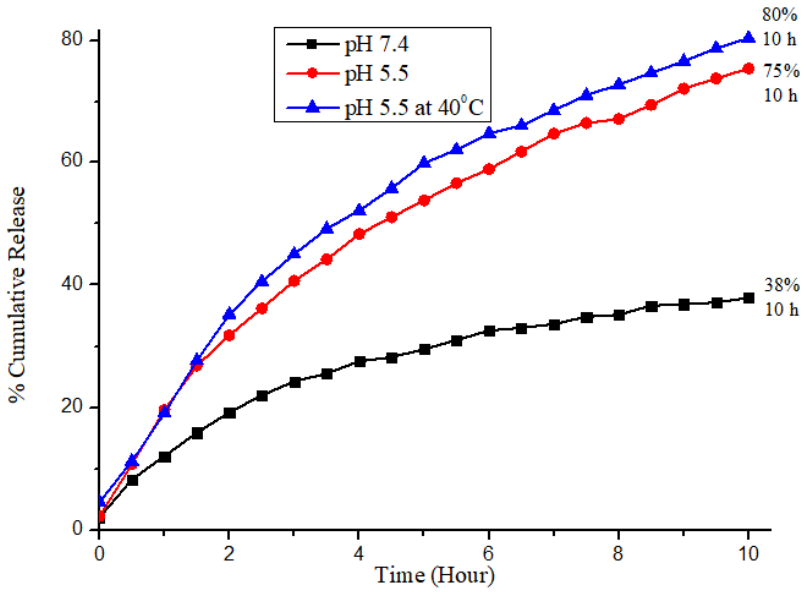

Figure. 3.18. Cumulative release profile of MTX from Octaminocryptand at pH 7.4 and pH 5.5.

To examine the release of MTX from octaminocryptand, we performed a cumulative release experiment of MTX at two different pH 7.4 (human physiological medium) and pH 5.5 (tumour environment) (figure 3.18). The release of MTX is observed in two stage: in first stage 23 % of the MTX is releasesed in 3 hours at pH 7.4 followed by a controlled release of around 38 % in next 7 hours at same pH. On the other hand, the release profile of MTX at acidic pH 5.5 showed a continuous release of MTX upto 75 % in 10 hours. It was observed that at any given time, a % release of MTX at pH 5.5 is higher as compare to the % release of MTX at pH 7.4. This behaviour supports the hypothesis that the said carrier will preferentially release MTX to

the cancerous cells which are known to have acidic pH. To explore the effect of temperature stimulus, we studied release of MTX at 40 °C. The % release of MTX from the octaminocryptand again increased with the temperature of sink volume around 40 °C as compare to release at room temperature. 80 % of the MTX is released from the octaminocryptand at 40 °C at pH 5.5. The microenvironment of cancerous cells is reported[43] to have slightly higher temperature as compare to microenvironment of normal cells. This further supports the preferential release of MTX at the tumour site.

The cytotoxicity of octaminocryptand, inclusion complex and MTX were investigated against MCF-7 and HeLa cell lines. There was no cytotoxic effect of octaminocryptand on MCF-7 and almost 100% cell viability was found up to 300 μM concentration of octaminocryptand, while significant cytotoxicity was observed with IC_{50}=0.3 μM on HeLa cells. The cytotoxicity of octaminocryptand on HeLa cell line revealed the self-therapeutic behaviour of octaminocryptand (table 3.2).

The IC_{50} value of inclusion complex of octaminocryptand loaded with MTX was found to be 117.26 μM and 16.84 μM on MCF-7 and HeLa cell line respectively. The enhanced cytotoxicity of inclusion complex as compared to the free drugs reveals the preferential entry of MTX in the cancerous cells in form of an inclusion complex. The synergistic effect of inclusion complex can also be attributed to self-therapeutic effect of octaminocryptand in case of HeLa cells.

Sr. No.	**Compound**	**IC_{50} (MCF-7) (μM)**	**IC_{50} (Hela) (μM)**
1.	Octaminocryptand	>300	0.3 ± 0.24
2.	Methotrexate ⊂ Octaminocryptand	117.26±23.87	16.847± 4.47
3.	Methotrexate	211.52±8.72	94.186±8.790

Table. 3.2. Cytotoxicity of octaminocryptand, inclusion complex and MTX against MCF-7 and HeLa cancer cells for 24 hours incubation by MTT assay.

To evaluate the acute oral toxicity of octaminocryptand, inclusion complex and MTX, male and female wistar rats were administered dosages through oral route. The animals were

observed individually for any sign of changes in behavior and physiological appearance with special attention during the first 4 h, then periodically during the 24 h. All the animals were observed for signs of toxicity, morbidity and mortality for 14 days .Observations were focused on determining any signs of toxicity, such as changes in skin and fur, eyes and mucous membranes, and also respiratory, circulatory, autonomic and central nervous systems, and somatomotor activity and behavior pattern. Attention should be directed to observations of tremors, convulsions, salivation, diarrhea, lethargy. At the end of the test, surviving animals were weighed, no significant weight loss was observed as compared to the initial weight on the 1st day. The animals were healthy and fit. There were no signals of toxicity in the animals treated with the inclusion complex as well as octaminocryptand. No changes were found in skin and fur, eyes, mucous membranes, and also respiratory, circulatory, autonomic, and central nervous system and convulsions, salivation, diarrhea, lethargy, sleep and coma. No death rate occurred during the test.

B. Flutamide (Ft)

The next drug we chose for binding with the cryptand from BCS class II is Flutamide. The nonsteroidal antiandrogen flutamide (FL) is therapeutically useful for the treatment of benign prostatic hypertrophy and androgen-dependent prostate cancer[44]. The inclusion of flutamide (Ft) with octaminocryptand was prepared by the kneading method. The inclusion complex was characterized by FT-IR, NMR, UV and DSC techniques. There is a change in the stretching frequencies of Ft after getting encapsulated in the cryptand as revealed by FT-IR spectrum (spectrum 3.15 and 3.16). The UV absorption peak of cryptand showed hypsochromic and hyperchromic shift after the encapsulation of Ft (figure 3.19).

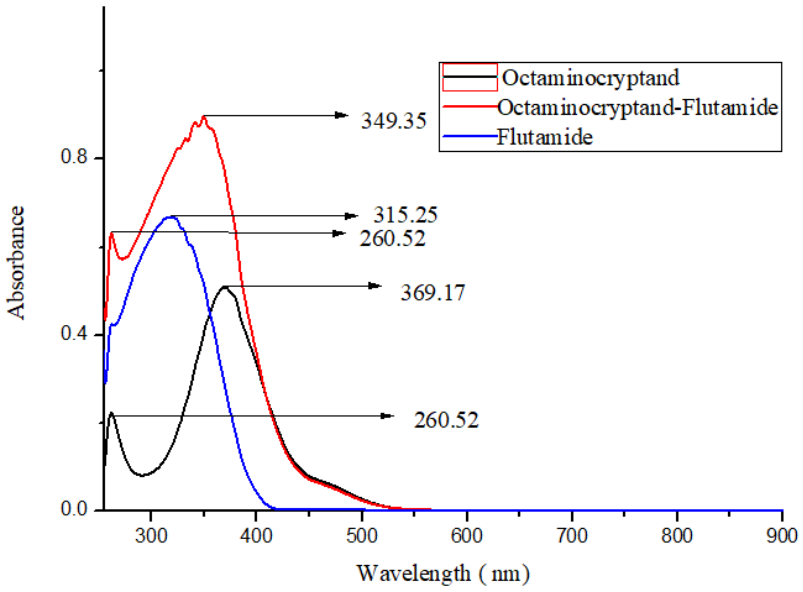

Figure. 3.19. UV-Vis absorption spectra of octaminocryptand, inclusion complex and flutamide.

The ^{1}H NMR titration of flutamide with octaminocryptand gives further insight about the interactions between them.

The protons of Ft gives three signals in aromatic region and two in aliphatic region (spectrum 3.17). The amide proton of Ft appears at 10.649 ppm, aromatic proton ortho to $-CF_3$ group appears at 8.311 ppm, aromatic proton ortho to nitro group appears at 8.200 ppm and the aromatic proton para to $-CF_3$ group appears at 8.068 ppm. The aliphatic proton of Ft appears at 2.652 ppm and 1.139 ppm.

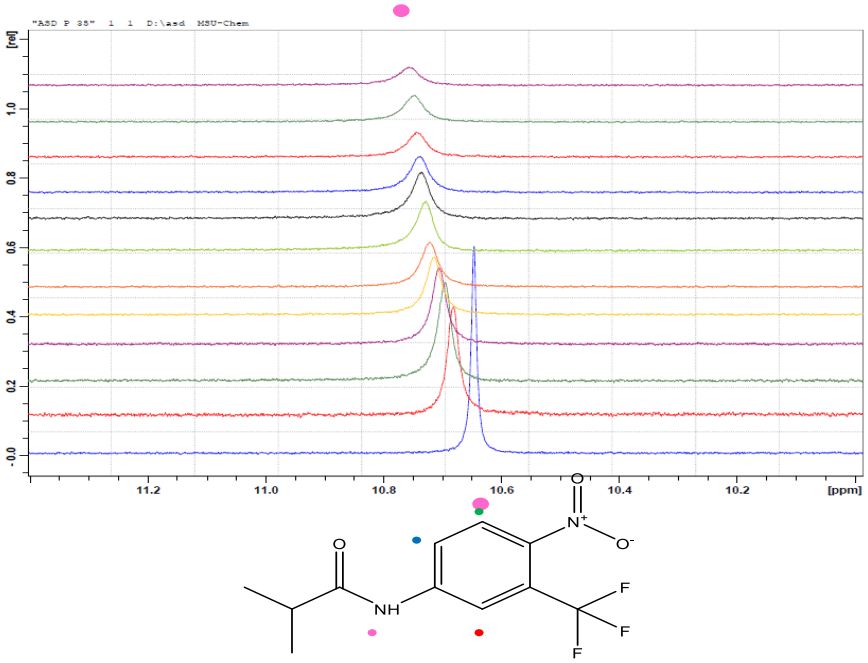

Figure. 3.20. Amide proton of Ft showed shifting in ^{1}H NMR titration with octaminocryptand.

In the^{1}H NMR titration the -NH proton of amide functionality of Ft gets shifted from 10.649 ppm to 10.778 ppm (figure 3.20). The aromatic proton ortho to $–CF_3$ group shifted from 8.311 ppm to 8.332 ppm. The aromatic proton ortho to nitro group shifted from 8.200 ppm to 8.203 ppm. The aromatic proton para to $-CF_3$ group shifted from 8.068 ppm to 8.084 ppm (figure 3. 21).

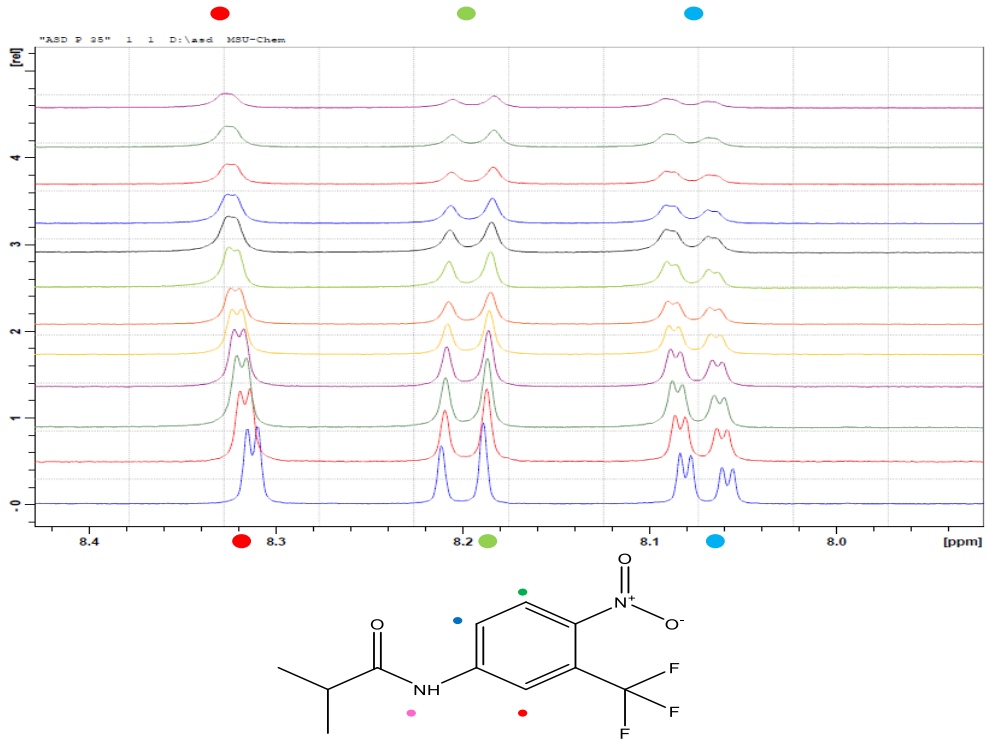

Figure. 3.21. Aromatic proton of Ft showed shifting in ^{1}H NMR titration with octaminocryptand.

The doublet due to methyl proton of Ft shifted from 1.139 ppm to 1.136 ppm (figure 3.22).

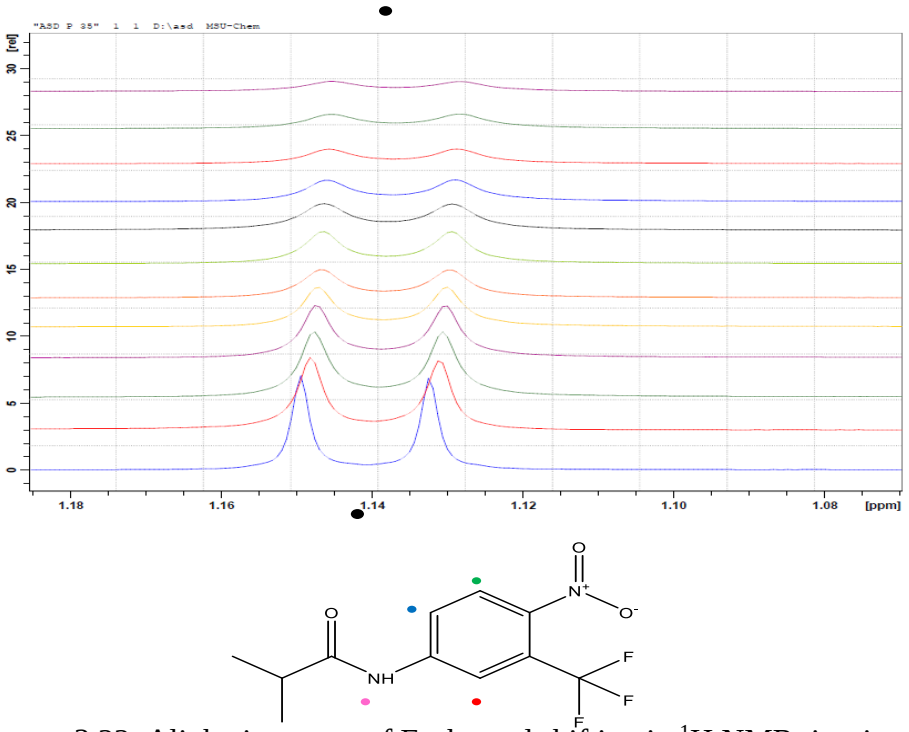

Figure. 3.22. Aliphatic proton of Ft showed shifting in ^{1}H NMR titration with octaminocryptand.

The drug loading capacity of octaminocryptand and encapsulation efficiency of Ft are found to be 43.37 % and 63.84 % respectively. The cumulative release profile of Ft at pH 5.5 showed 26 % release of Ft in 5 hours and controlled release of 35 % in 24 hours (figure 3.23).

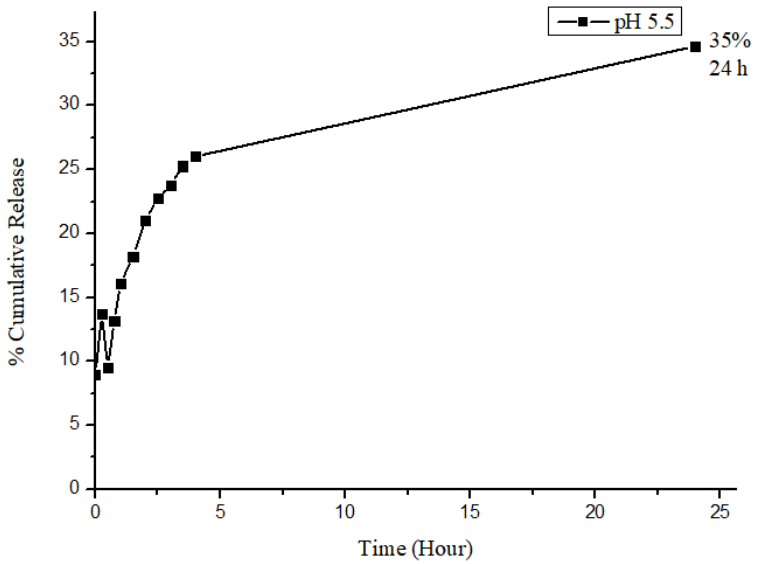

Figure. 3.23. Cumulative release profile of Ft from Octaminocryptand at pH 5.5.

The cytotoxicity of octaminocryptand, inclusion complex and flutamide were investigated against MDA-MB-231. The IC_{50} value of drug flutamide and octaminocryptand was found to be 71 µg/ml and 62 µg/ml respectively. The results suggest self-therapeutic behaviour of octaminocryptand on MDA-MB-231 cells (table 3.3).

The cytotoxicity was enhanced upon binding of flutamide with the octaminocryptand reflecting in the lower IC_{50} value of inclusion complex (53 µg/ml) as compared to free drug flutamide. The improved cytotoxicity of inclusion complex could be correlated to the capability of preferential internalization of flutamide loaded octaiminocryptand into the cells followed by sustained release of flutamide as well as the therapeutic efficacy of octaminocryptand exhibiting synergistic effect on cell viability.

Sr. No.	Compound	IC_{50} (MDA-MB-231) (μg/ml)
1.	Octaminocryptand	62 ± 1.2
2.	Flutamide ⊂ Octaminocryptand	53 ± 0.43
3.	Flutamide	71 ± 2.1

Table. 3.3. Cytotoxicity of octaminocryptand, inclusion complex and flutamide against MDA-MB-231 cancer cells for 24 hours incubation by MTT assay.

BCS class III

Gemcitabine hydrochloride (GEM)

As a single agent or in combination with other chemotherapeutic drugs, gemcitabine hydrochloride is a BCS class III drug of preference in the treatment of cancer. However, due to its brief half-life, its bioavailability is a significant concern[45]. The inclusion of GEM with the octaminocryptand was prepared by the kneading method. The inclusion complex was characterized by FT-IR and NMR techniques. There is a change in the stretching frequencies of GEM after getting encapsulated in the octaminocryptand as revealed by FT-IR spectrum (spectrum 3.18 and 3.19).

The ^{1}H NMR titration of GEM with octaminocryptand gives further insight about the interactions between them.

The protons of GEM gives five signals in aromatic region and four in aliphatic (spectrum 3.20). The proton of -OH group of furanose ring of GEM appears at 9.790 ppm and 8.718 ppm. The proton of nucleobase ring appears at 8.124 ppm and 6.202 ppm while the methylene proton of furanose ring appears at 6.079 ppm, 4.190 ppm and 3.645 ppm. The methylene proton neighbouring to –OH group appears at 3.912 ppm and 3.792 ppm.

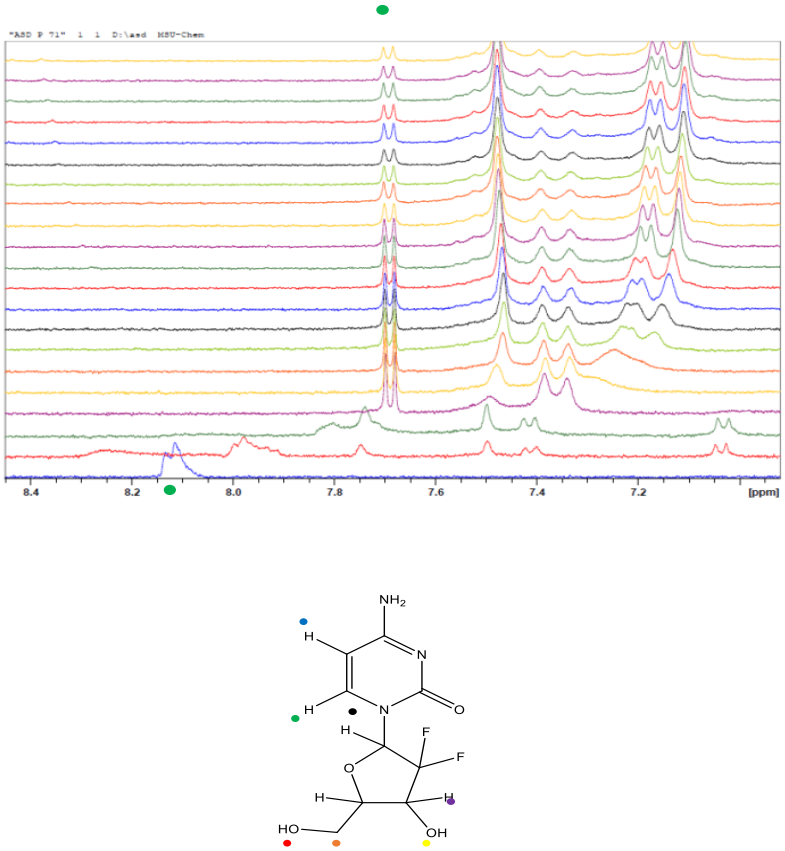

Figure. 3.24. Aromatic proton meta to amino group of GEM showed shifting in ^{1}H NMR titration with octaminocryptand.

From the ^{1}H NMR titration of GEM against the cryptand, it is observed that the aromatic proton meta to amino group of GEM shifted from 8.124 ppm to 7.685 ppm (figure 3.24) and other aromatic proton ortho to amino group of GEM shifted from 6.202 ppm to 5.787 ppm. The proton of furanose ring of GEM shifted from 6.079 ppm to 6.128 ppm (figure 3.25). This ^{1}H NMR titration showed a crossover of peaks of aromatic proton ortho to amino group and methine proton of carbon attached to nitrogen in the region of 6.2-5.7 ppm.

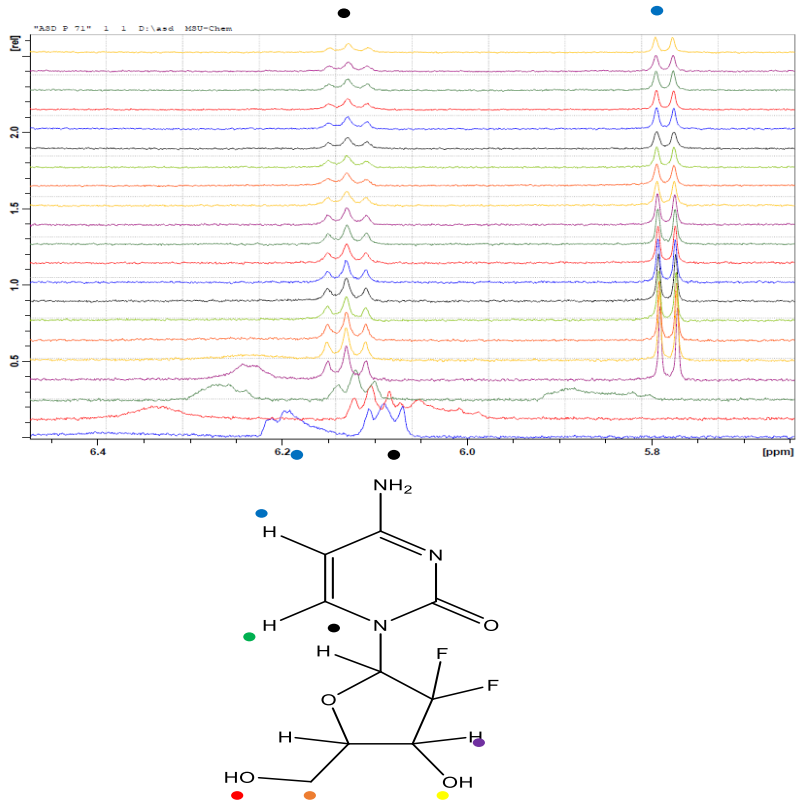

Figure. 3.25. Aromatic proton ortho to amino group of GEM and proton of furanose ring showed shifting in ^{1}H NMR titration with octaminocryptand.

The drug loading capacity of octaminocryptand and encapsulation efficiency of GEM are found to be 50.15 % and 71.46 % respectively. The cumulative release profile of GEM from octaminocryptand at two different pH 7.4 and 5.5 shows that at pH 7.4 the drug release is approximately negligible in amount while at pH 5.5 drug releases in two stages. In first stage 42.99 % drug is released continuously in 3 days and after 3 days the drug is released in controlled manner and a cumulative release of 46.20 % was observed within 5 days (figure 3.26).

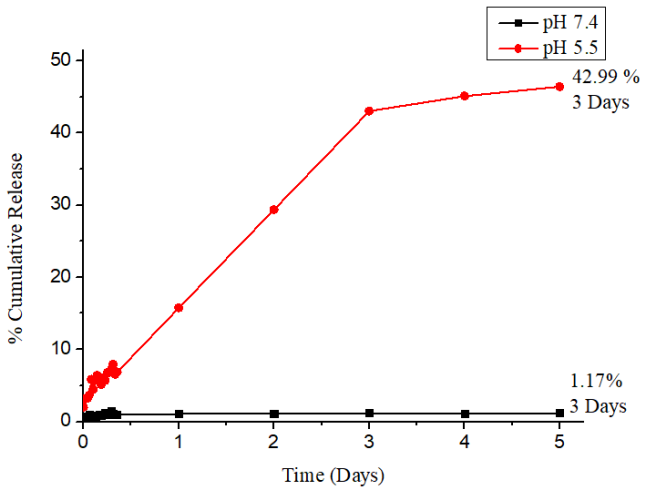

Figure. 3.26. Cumulative release profile of GEM from Octaminocryptand at pH 7.4 and pH 5.5.

The cytotoxicity of gemcitabine hydrochloride loaded octaminocryptand was investigated against MDA-MB-231. The IC_{50} value of inclusion complex was found to be 47 µg/ml which is better as compared to free drug gemcitabine hydrochloride (table 3.4).

Sr. No.	**Compound**	**IC_{50} (MDA-MB-231) (µg/ml)**
1.	Octaminocryptand	62 ± 1.2
2.	Gemcitabine hydrochloride ⊂ Octaminocryptand	47 ±0.091
3.	Gemcitabine hydrochloride	51 ± 0.65

Table. 3.4. Cytotoxicity of octaminocryptand, inclusion complex and gemcitabine hydrochloride against MDA-MB-231 cancer cells for 24 hours incubation by MTT assay.

3.4. Conclusion

We have synthesized a curcuminoid based hexaiminocryptand from high dilution method. The selective reduction of imine bond enhances the aqueous solubility and flexibility of the system. We chose three drugs to incorporate with octaminocryptand: methotrexate, flutamide and gemcitabine hydrochloride. The interaction between the octaminocryptand and drugs were investigated through various techniques including NMR titrations and NOESY. We observed a pH triggered sustained release of all three drugs from octaminocryptand. The cell viability study through MTT assay against various cell line such as MCF-7, HeLa and MDA-MB-231 revealed the self-therapeutic behavior of octaminocryptand and synergistic cytotoxic effect of inclusion complexes. The synergistic cytotoxic effect might be correlated with the selective escort of encapsulated drug through the cancer cell membrane as well as therapeutic effect of the carrier on cancer cells. However, using inclusion complexes of drug with supramolecular carriers overcome the transporter mediated multidrug resistant due to the passing through of supramolecular carriers through the cellular membrane and releasing the drug in a sustained manner[76]. In vivo acute oral toxicity studies showed that there were no toxicity of octaminocryptand and inclusion complex on healthy wistar rats.

3.5 Analytical Data

Spectrum 3.1: FT-IR spectrum of Hexaiminocryptand

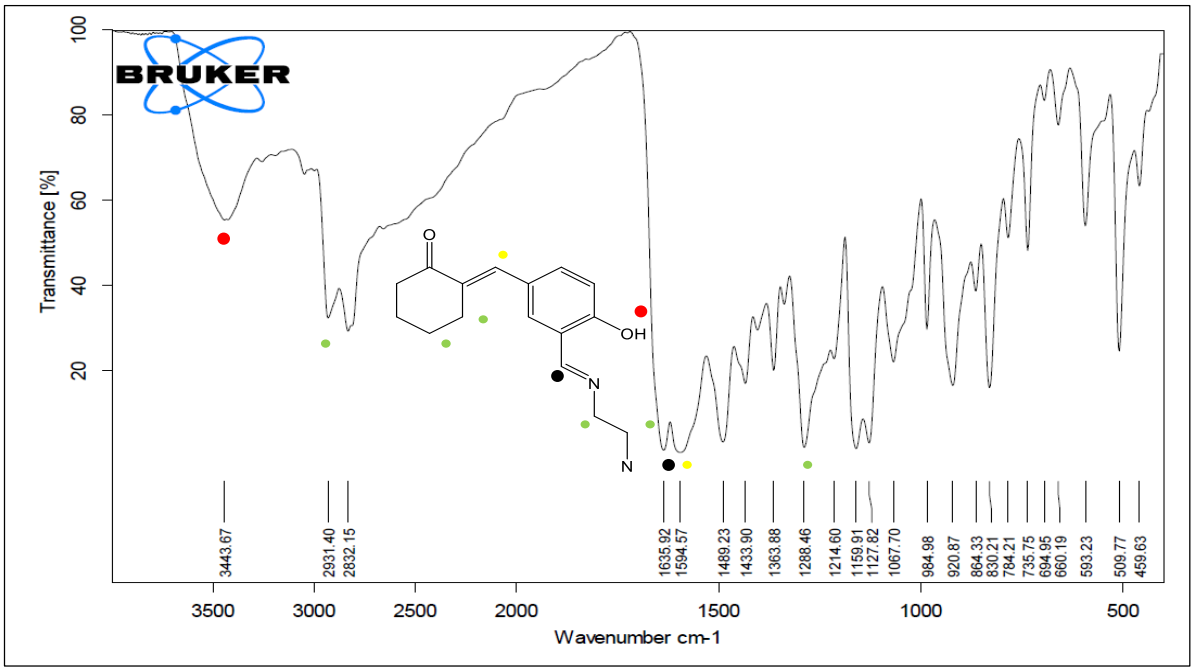

Spectrum 3.2: ^{1}H NMR spectrum of Hexaiminiocryptand

$CDCl_3$

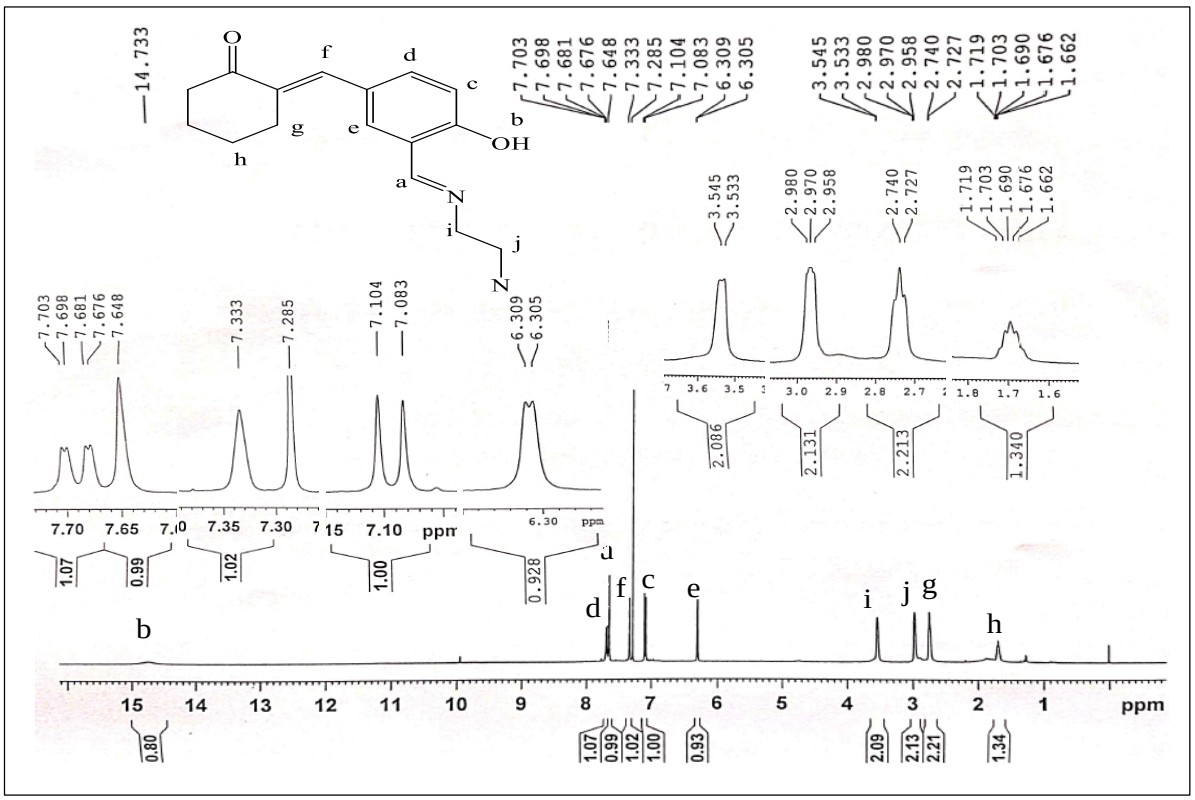

Spectrum 3.3: ^{13}C NMR spectrum of Hexaiminocryptand

$CDCl_3$

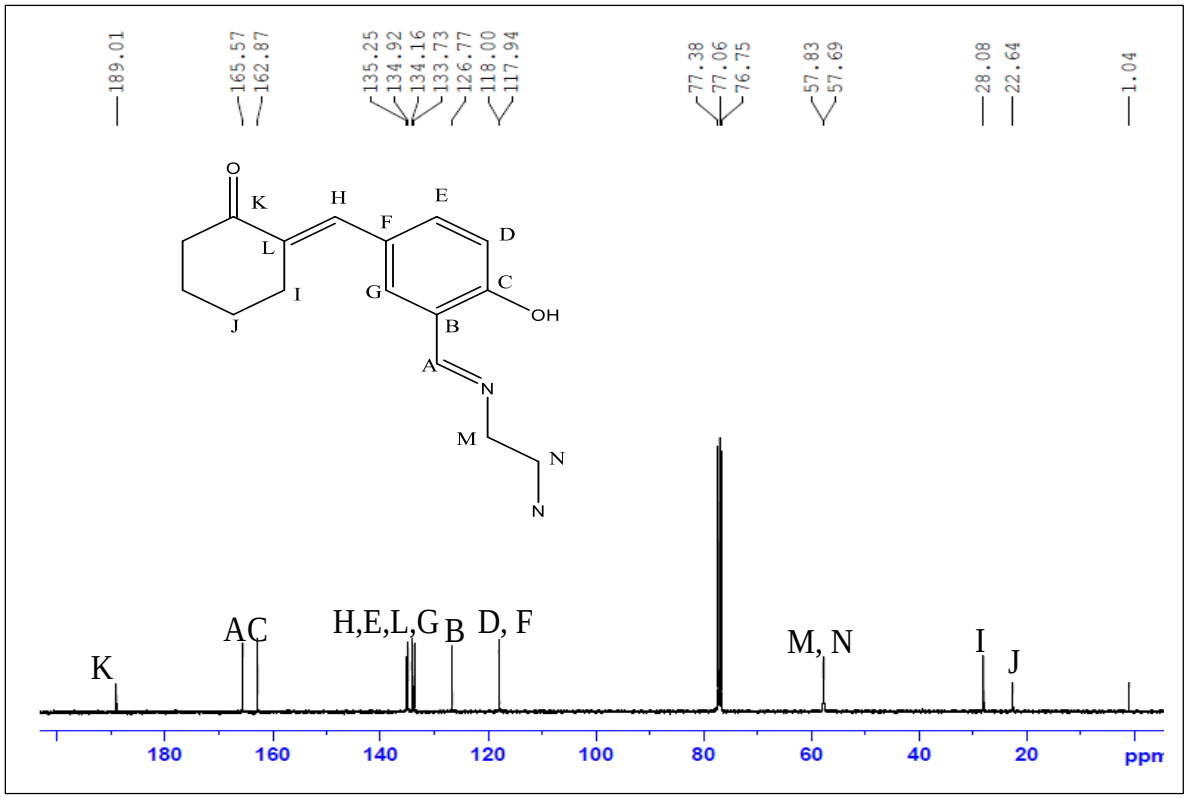

Spectrum 3.4: 135 DEPT NMR spectrum of Hexaiminocryptand

$CDCl_3$

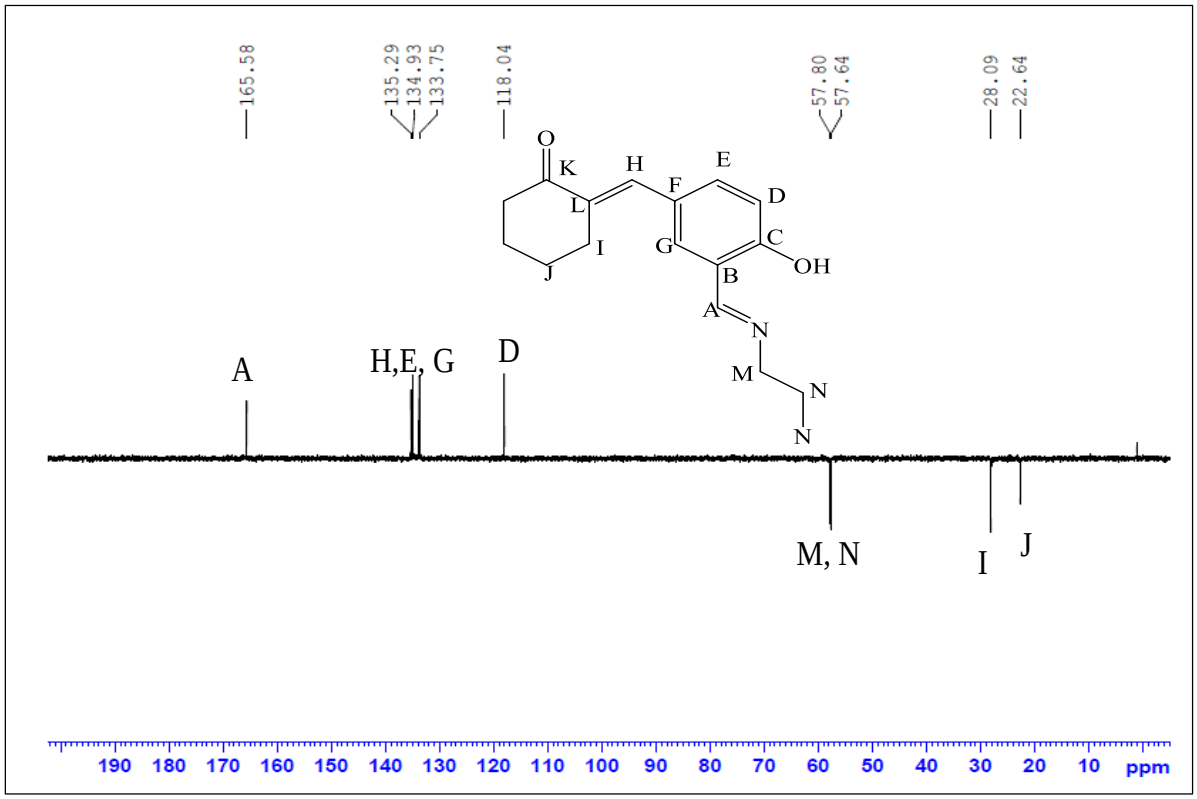

Spectrum 3.5: HR-MS spectrum of Hexaiminocryptand

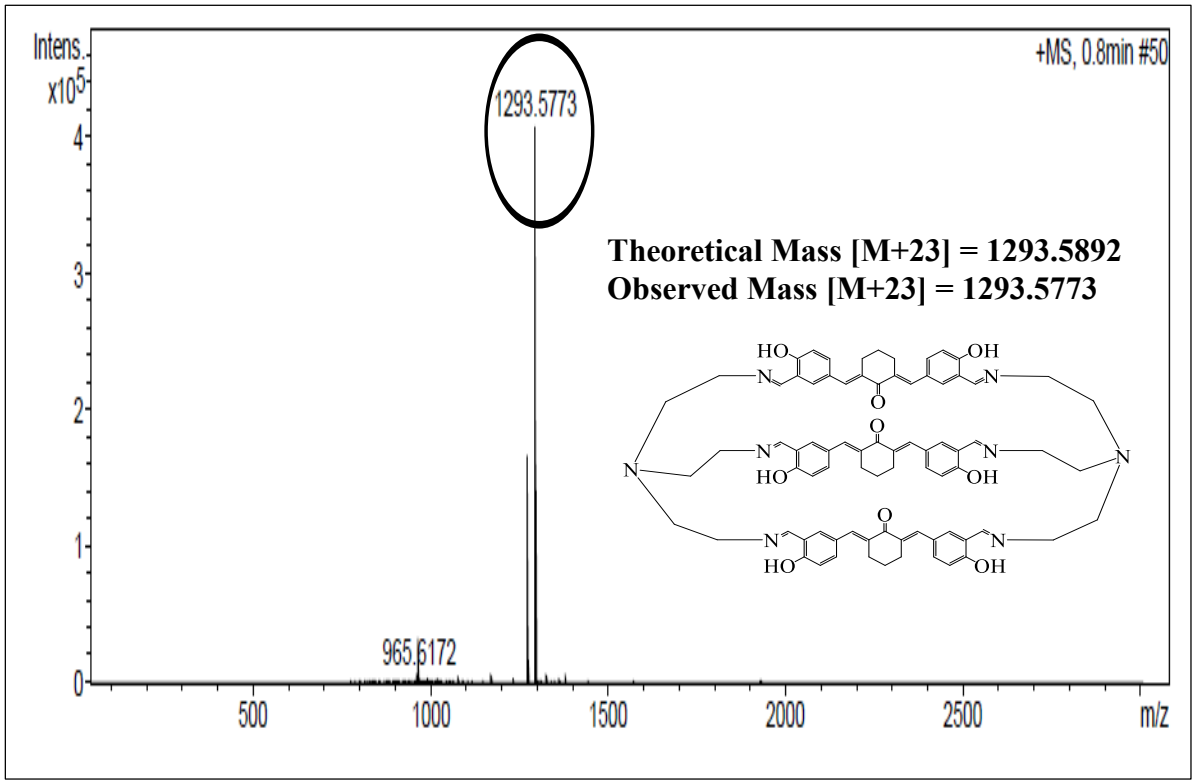

Spectrum 3.6: FT-IR spectrum of Octaminocryptand

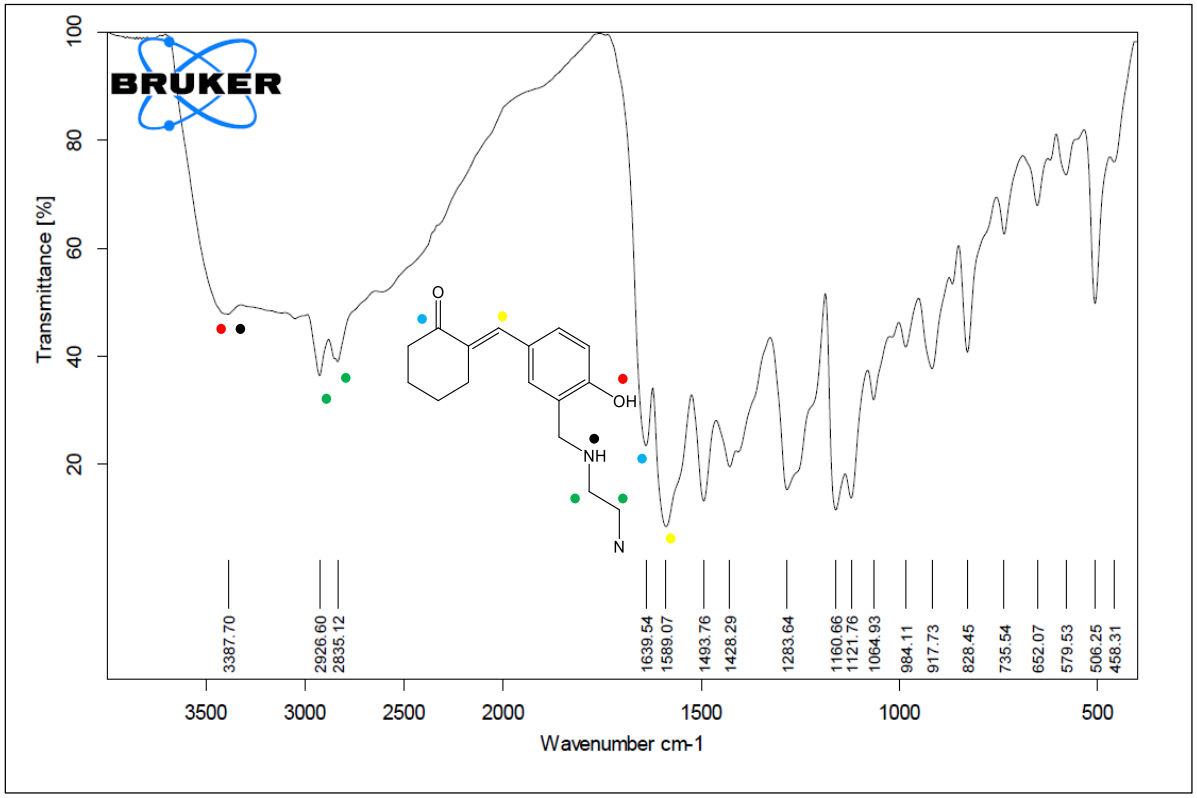

Spectrum 3.7: ^{1}H NMR spectrum of Octaminocryptand

DMSO-d_6

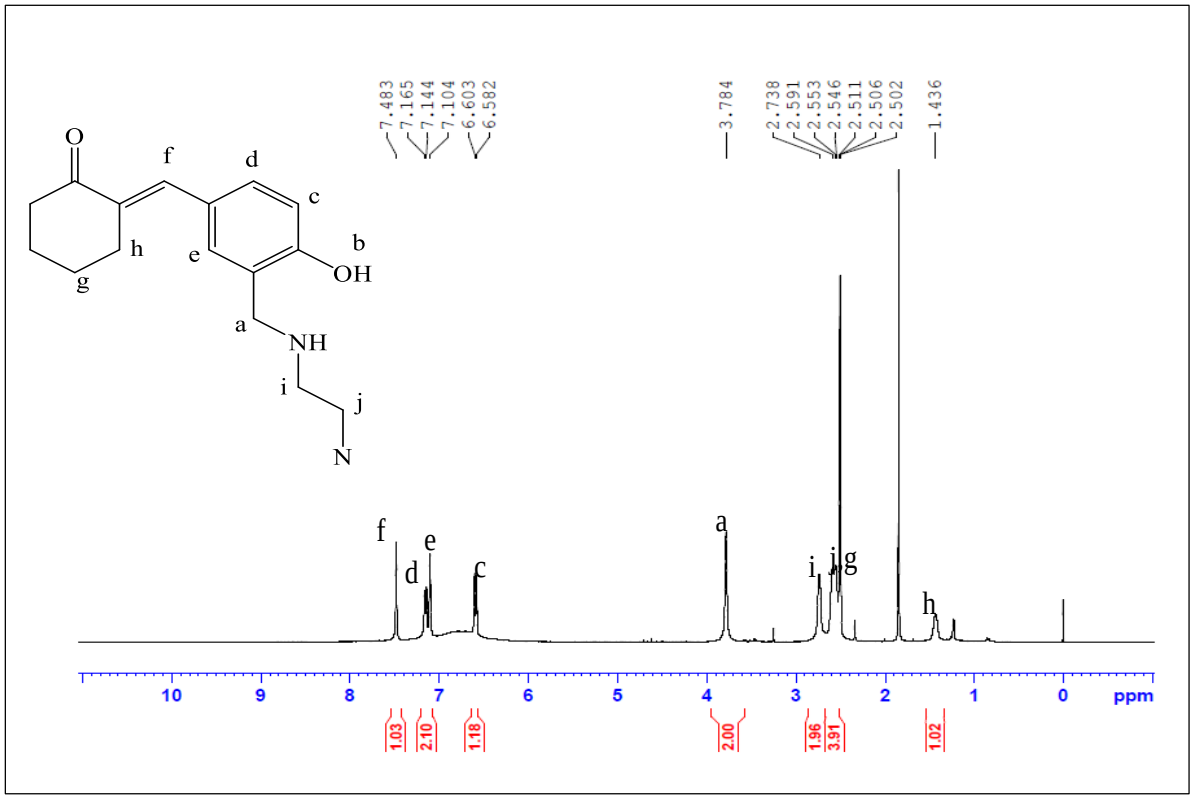

Spectrum 3.8: ^{13}C NMR spectrum of Octaminocryptand

DMSO-d_6

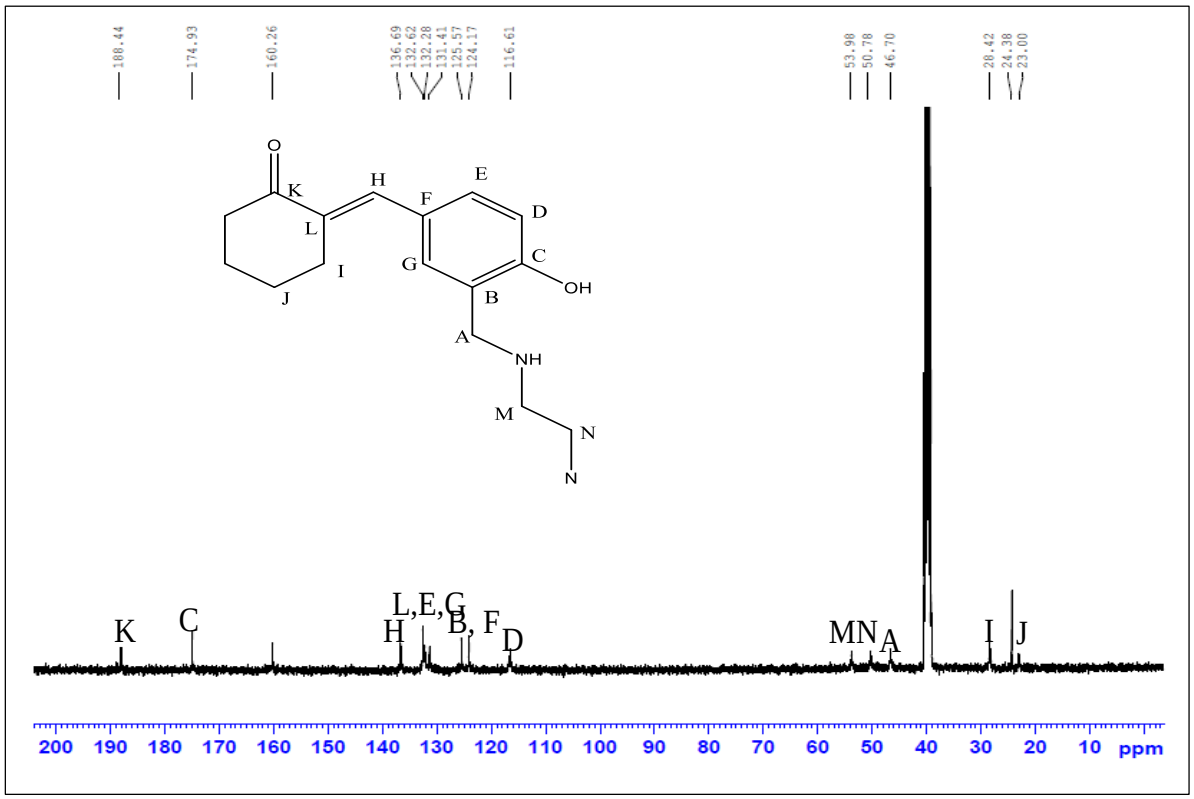

Spectrum 3.9: 135 DEPT NMR spectrum of Octaminocryptand

DMSO-d_6

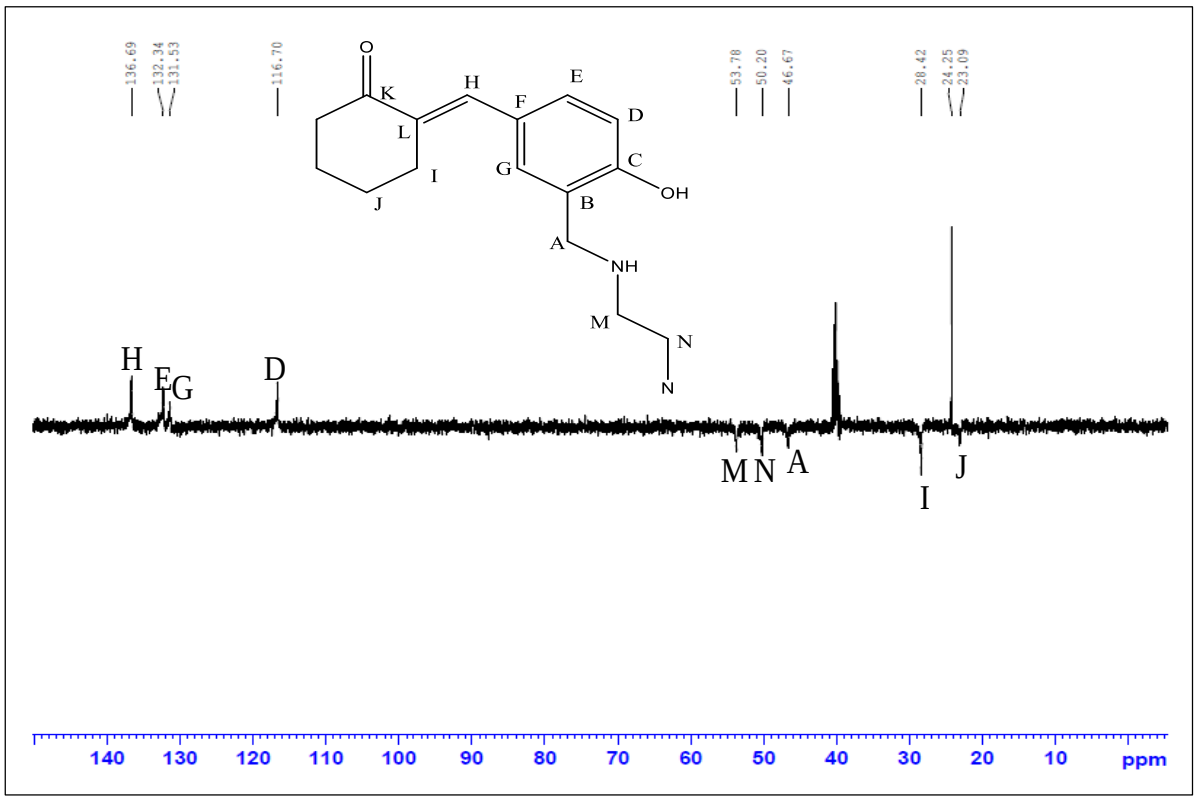

Spectrum 3.10: HR-MS spectrum of Octaminocryptand

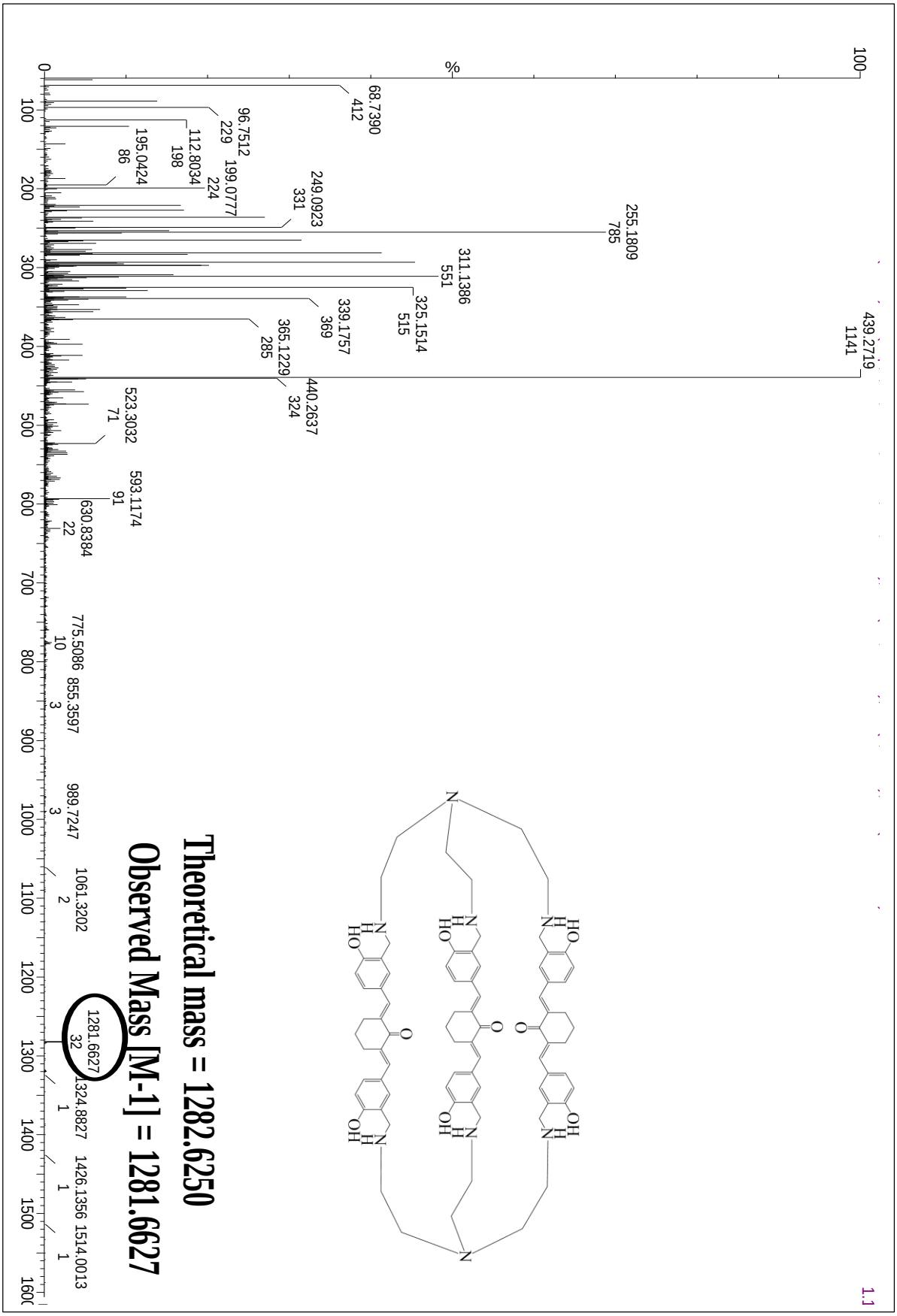

Spectrum 3.11: FT-IR spectrum of Methotrexate loaded Octaminocryptand

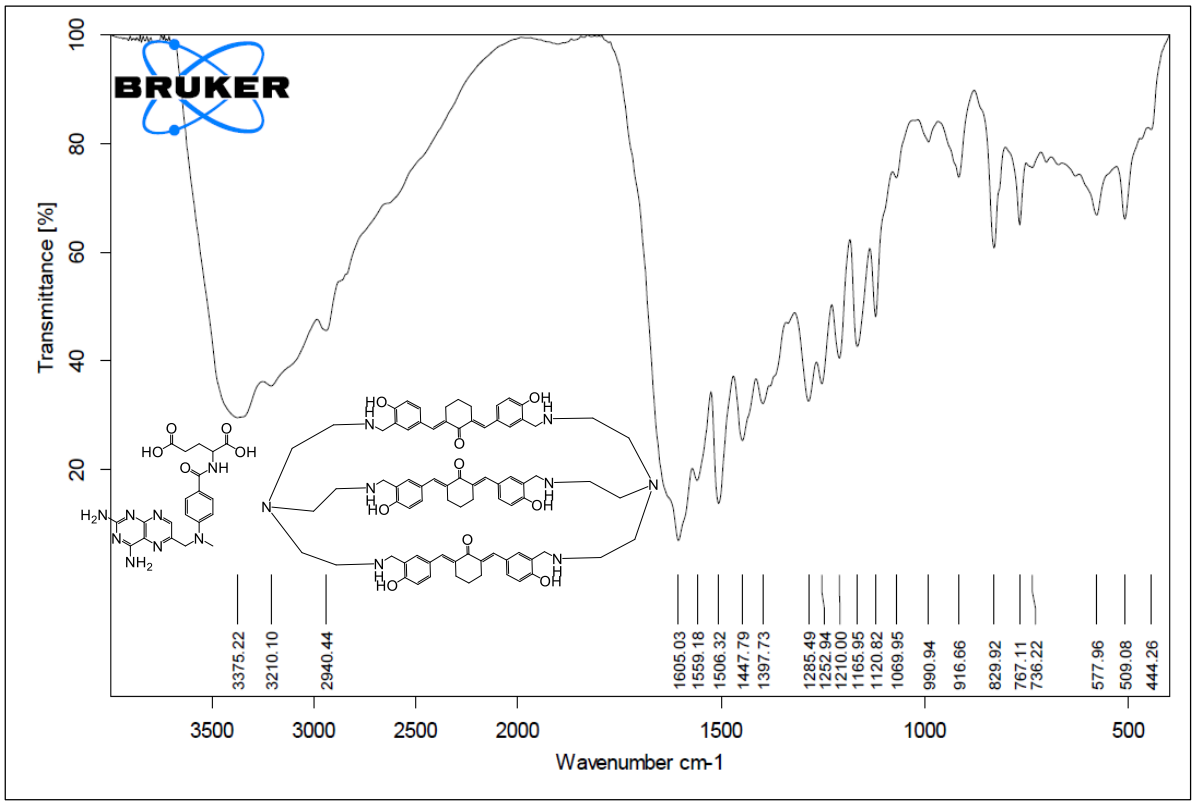

Spectrum 3.12: FT-IR spectrum of Methotrexate

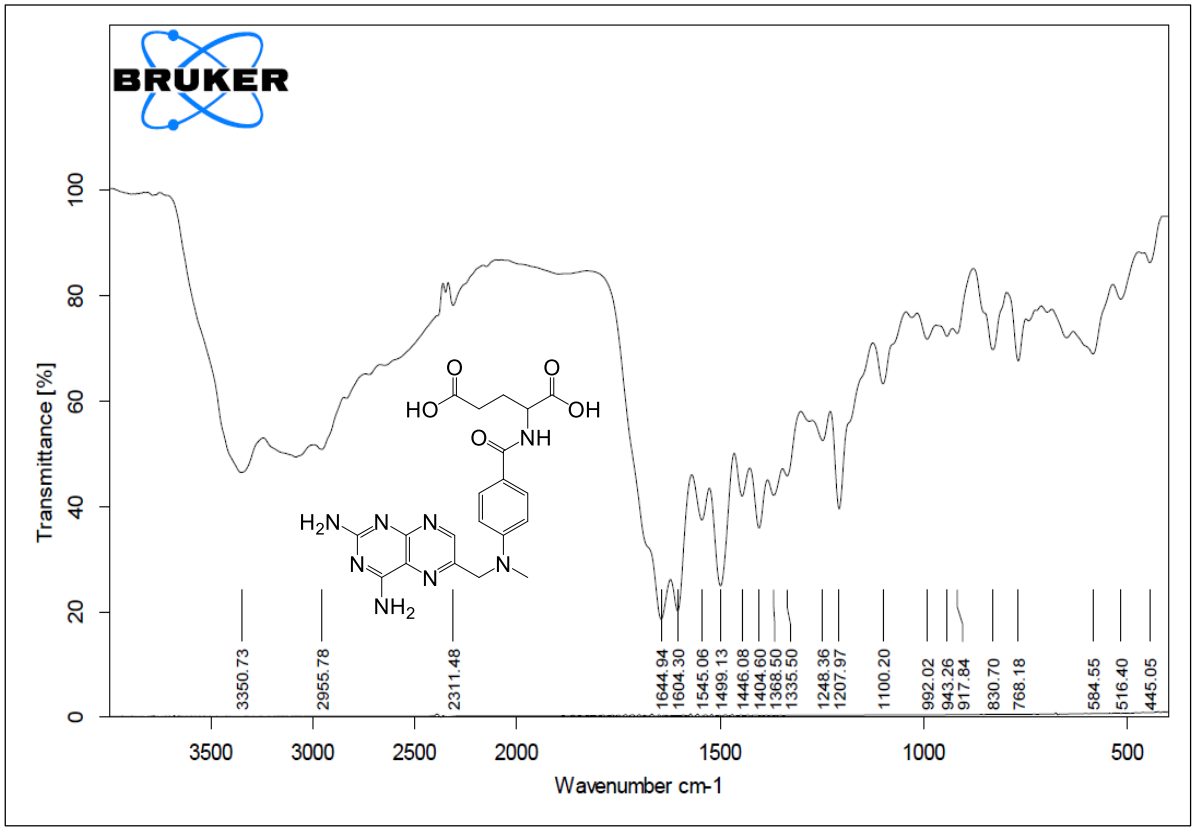

Spectrum 3.13: ^{1}H NMR spectrum of Methotrexate **DMSO-d$_6$**

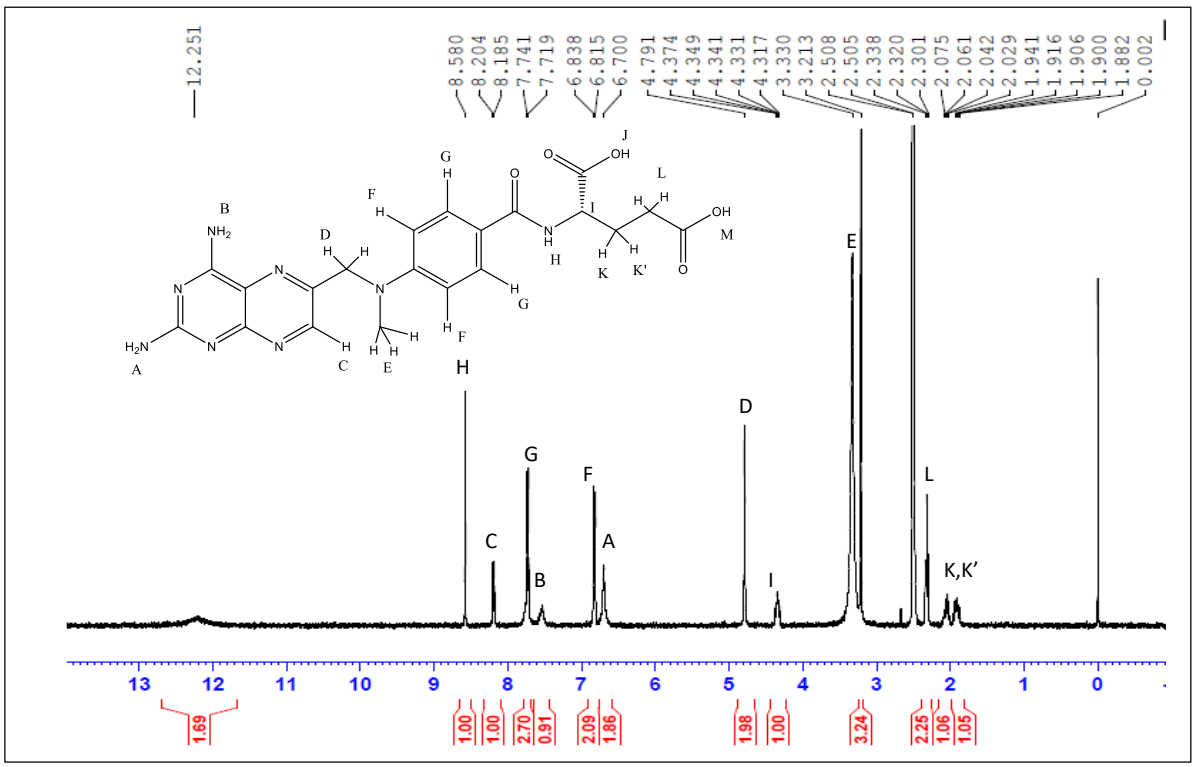

Spectrum 3.14: ^{1}H NMR spectrum of Methotrexate loaded Octaminocryptand **DMSO-d$_6$**

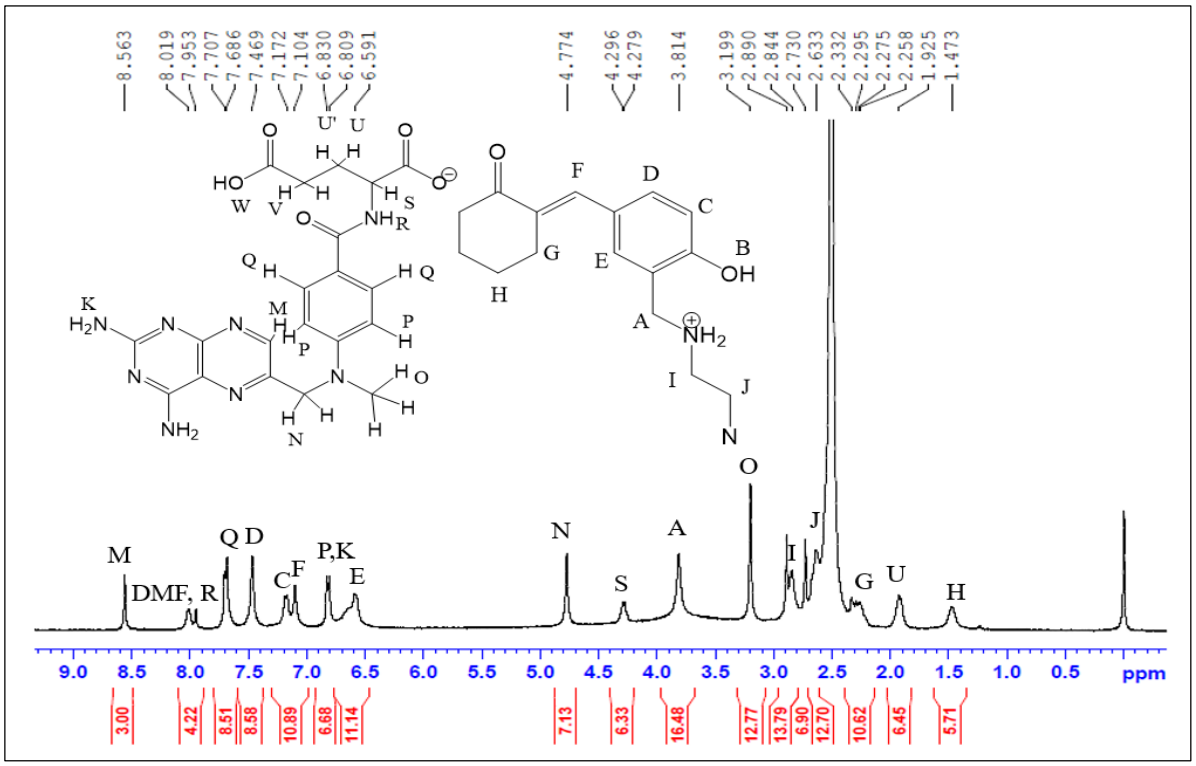

Spectrum 3.15: FT-IR spectrum of Flutamide loaded Octaminocryptand

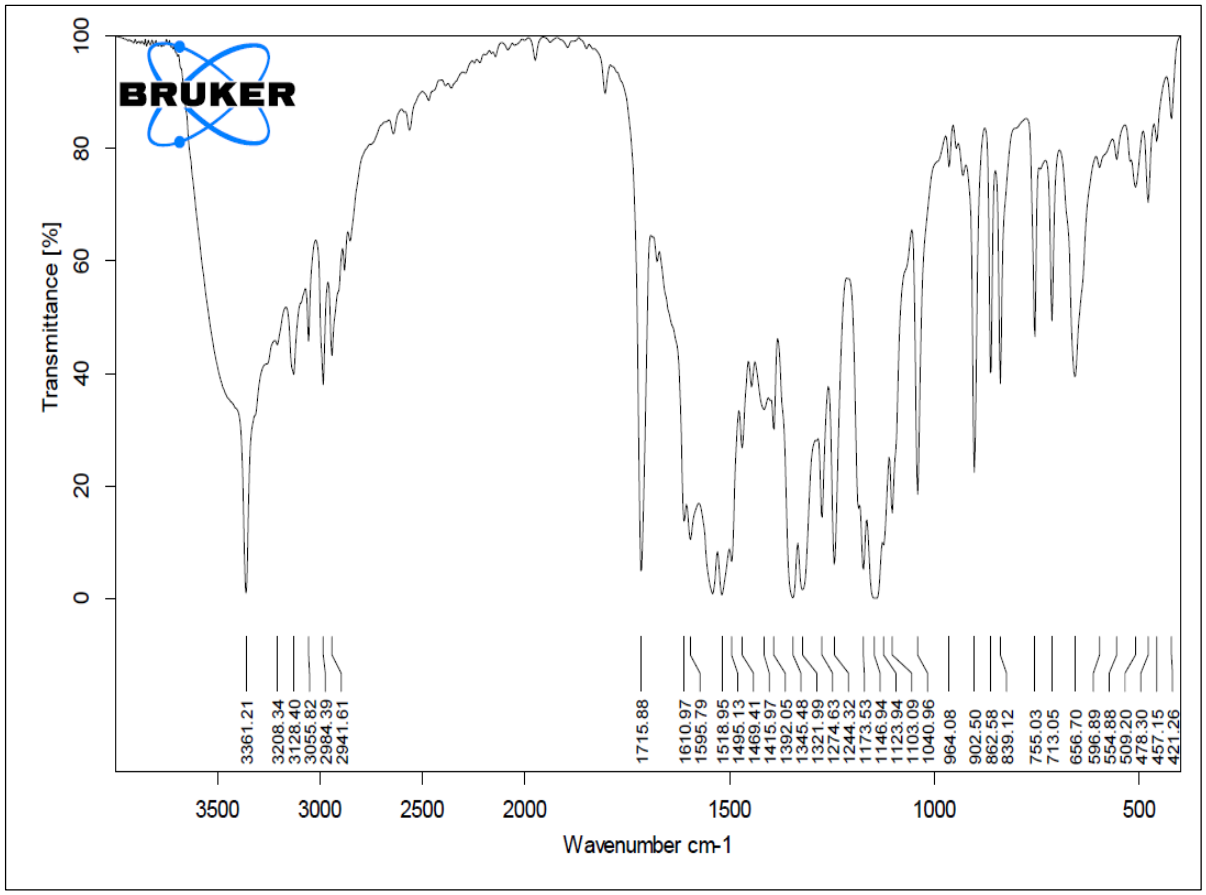

Spectrum 3.16: FT-IR spectrum of Flutamide

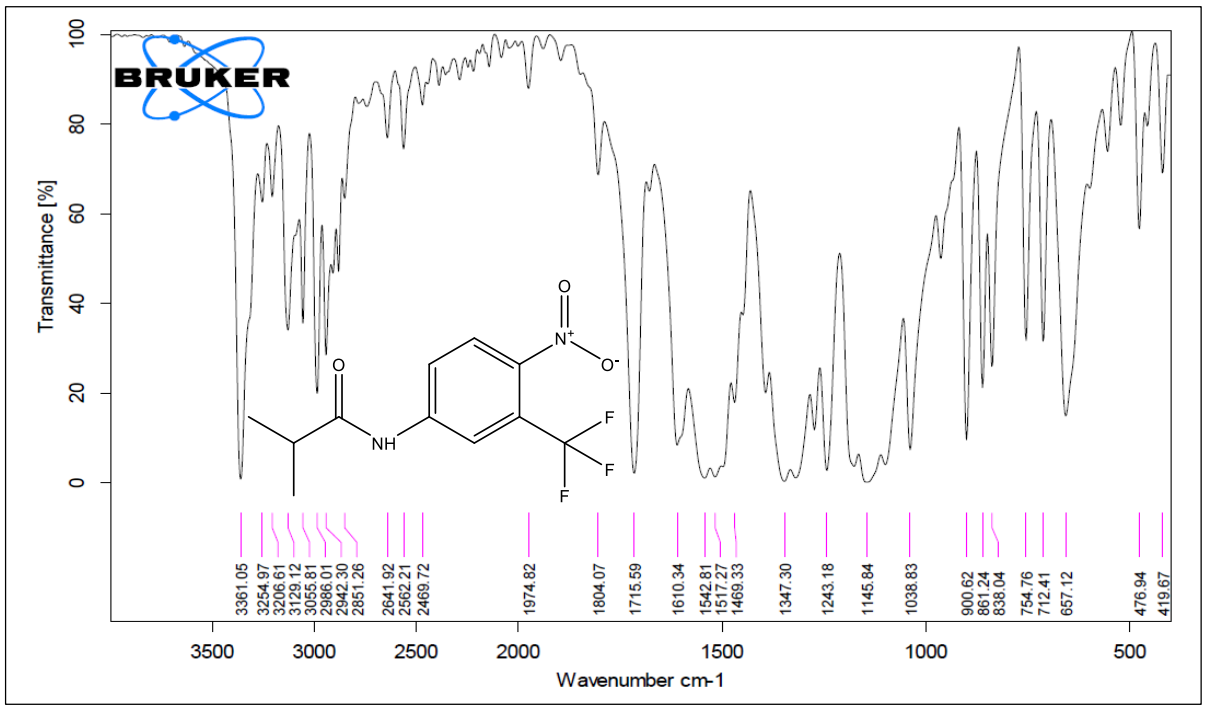

Spectrum 3.17: ^{1}H NMR spectrum of Flutamide **DMSO-d_6**

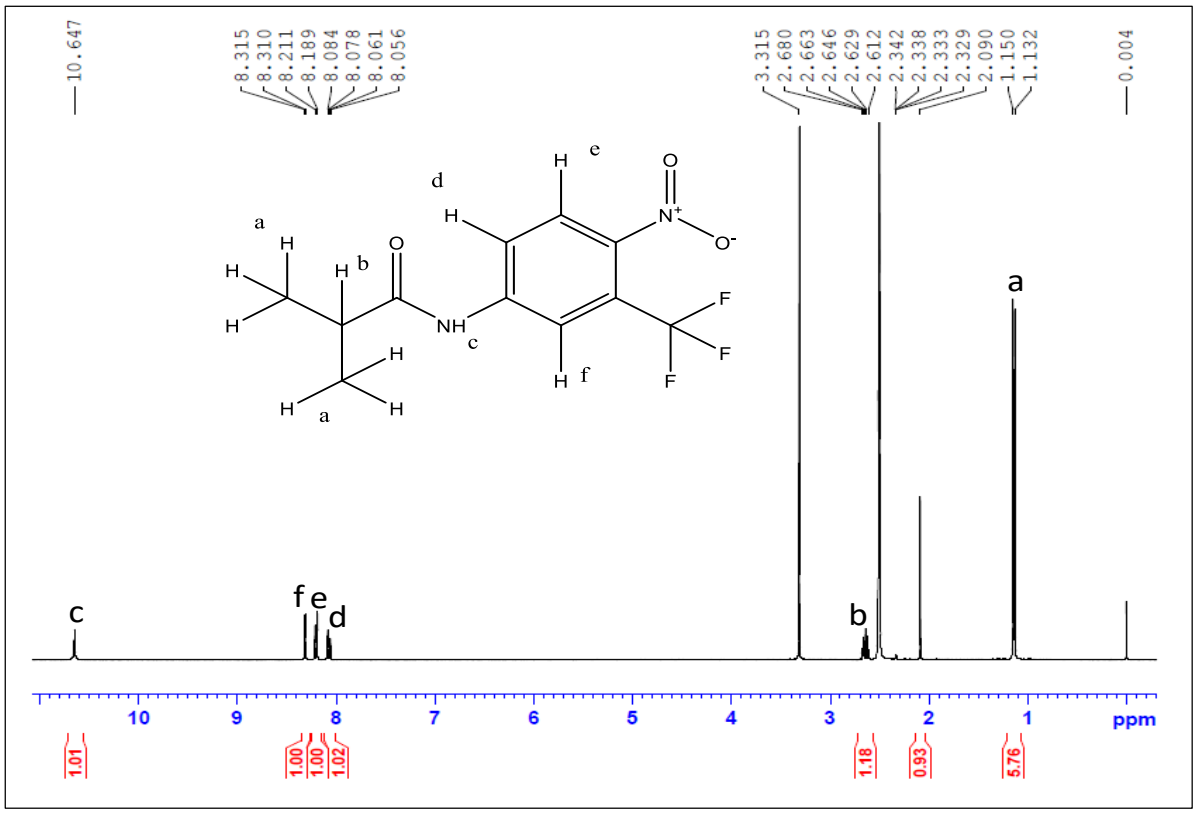

Spectrum 3.18: FT-IR spectrum of Gemcitabine hydrochloride loaded Octaminocryptand

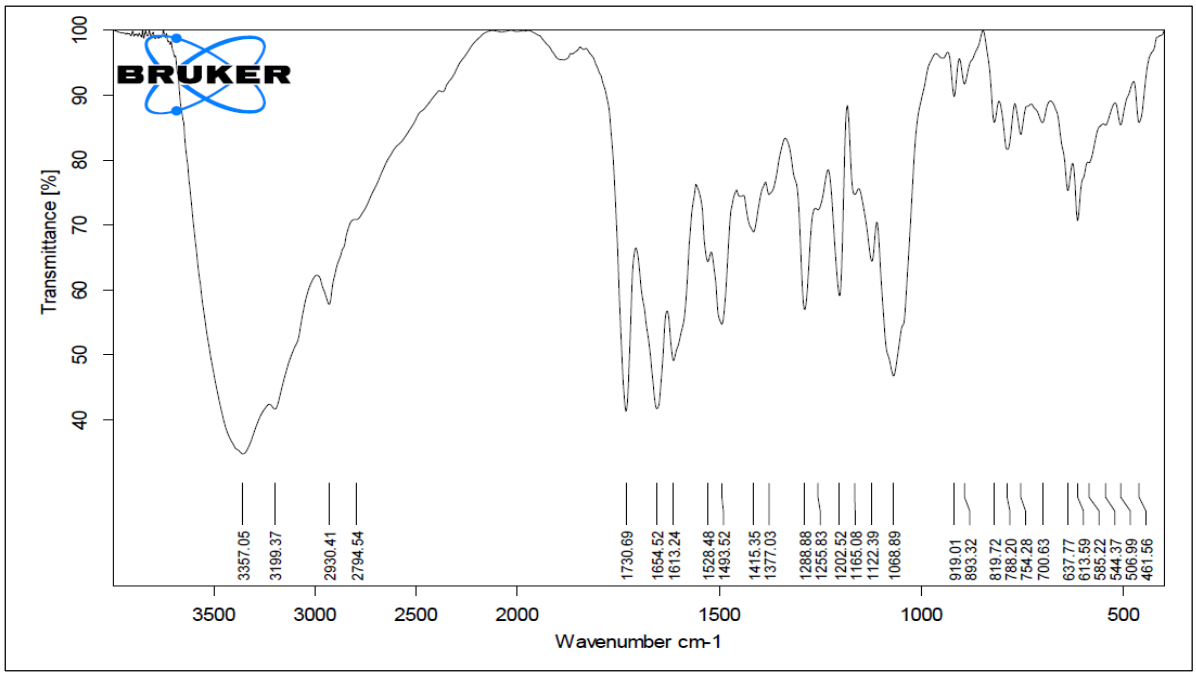

Spectrum 3.19: FT-IR spectrum of Gemcitabine Hydrochloride

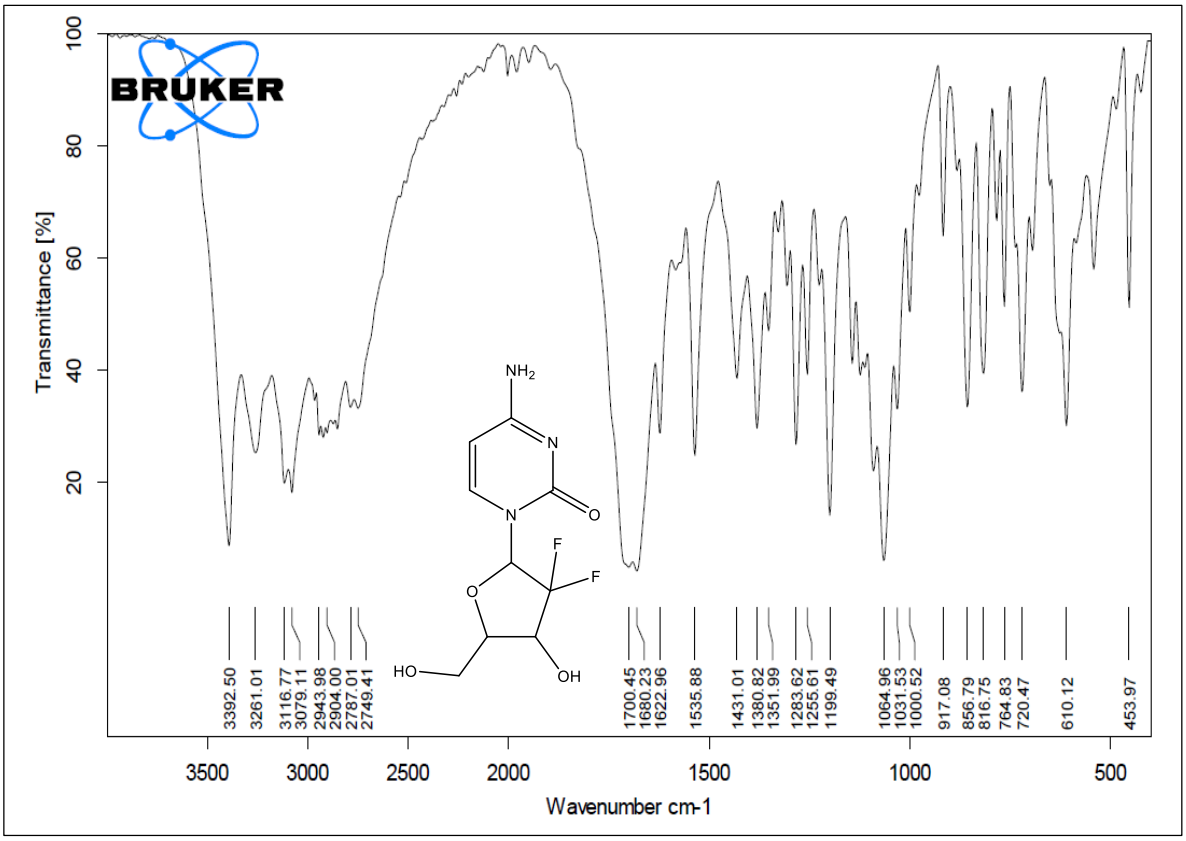

Spectrum 3.20: ^{1}H NMR spectrum of Gemcitabine Hydrochloride

DMSO-d$_6$

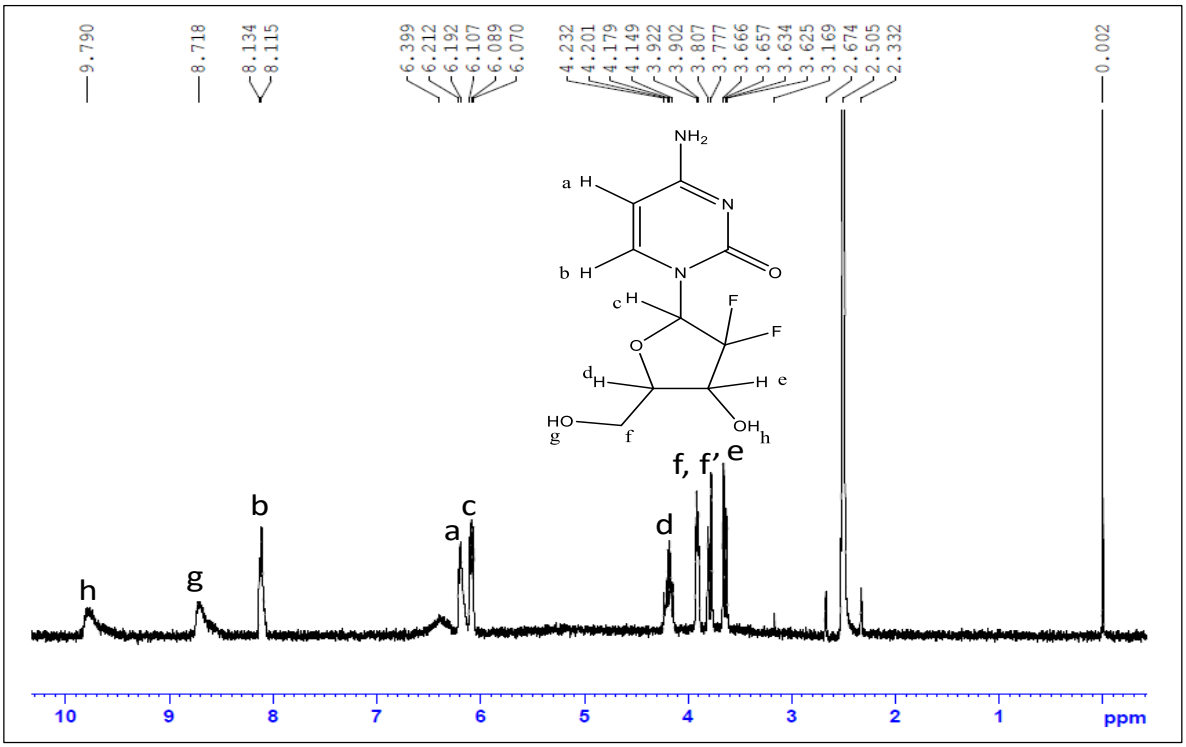

3.6. References

1 H. E. Simmons, C. H. Park, *J. Am. Chem. Soc.*, 1968, **90**, 2428–2429.

2 H. E. Simmons, C. H. Park, *J. Am. Chem. Soc.*, 1968, **90**, 2429–2431.

3 H. E. Simmons, C. H. Park, *J. Am. Chem. Soc.*, 1968, **90**, 2431–2432.

4 B. Dietrich, J. M. Lehn, J. P. Sauvage, *Tetrahedron Lett.*, 1969, **34**, 2889–2892.

5 S. K. Menon, S. V. Hirpara, U. Harikrishna, *ChemInform*, 2004, **23**, 233–267.

6 A. S. Braegelman, M. J. Webber, *Theranostics*, 2019, **9**, 3017-3040.

7 R. C. Brachvogel, F. Hampel and M. V. Delius, *Nat. Commun.*, 2015, **6**, 1–7.

8 M. Zhang, X. Yan, F. Huang, Z. Niu, H. W. Gibson, *Acc. Chem. Res.*, 2014, **47**, 1995-2005.

9 A. W. Mcdonagh, B. L. Mcneil, B. O. Patrick, C. F. Ramogida, Inorg. Chem., 2021, 60, 10030-10037.

10 J. Jazwinski, J. M. Lehn, D. Lilienbaum, R. Ziessel, J. Guilhem, C. Pascard, *J. Chem. Soc. Chem. Commun.*, 1987, 1691-1694.

11 M. Moder, K. Wichmann, K. Gloe, F. Vogtle, *Int. J. Mass. Spectrom.*, 2001, **210-211**, 327-339.

12 D. E. Fenton and B. A. Najera, *J. Coord. Chem.*, 2001, **54**, 239-246.

13 S. O. Kang, M. Llinares, D. Powell, D. Vandervelde and K. B. James, J. *Am. Chem. Soc.*, 2003, **125**, 10152–10153.

14 S. Kang, S. J. Lee, S. Yan, K. C. Nam, J. Y. Lee, *J. Inc. Phenom. Macrocycle. Chem.*, 2010, **66**, 75–79.

15 S. O. Kang, V. W. Day, K. B. James, *J. Org. Chem.*, 2010, **75**, 277-283.

16 Q. Q. Wang, R. A. Begum, V. W. Day and K. Bowman-james, *Polyhedron*, 2013, **52**, 515–523.

17 S. Brooker, J. D. Ewing, J. Nelson, *Inorganica Chim. Acta*, 2001, **317**, 53–58.

18 S. Brooker, J. D. Ewing, J. Nelson, J. C. Jeffery, *Inorganica Chim. Acta*, 2002, **337**, 463–466.

19 S. Brooker, J. D. Ewing, T. K. Ronson, C. J. Harding, J. Nelson, D. J. Speed, *Inorg. Chem.*, 2003, **42**, 2764-2773.

20 T. K. Ronson, J. Nelson, G. B. Jameson, J. C. Jeffery, S. Brooker, *Eur. J. Inorg. Chem.*, 2004, 2570-2584.

21 M. Kumar, V. J. Aran, P. Navarro, *Tetrahedron Lett.*, 1995, **36**, 2161–2164.

22 B. Cabezon, M. Irurzun, T. Torres, P. Vazquez, *Tetrahedron Lett.*, 1998, **39**, 1067–1070.

23 M. P. T. Fichou, J. P. Vigneron, J. M. Lehn, *J. Chem. Soc. Perkin Trans.*, 1996, **2**, 2169-2175.

24 A. E. Martell, R. J. Motekaitis, Q. Lu and D. A. Nation, *Polyhedron*, 1999, **18**, 3203–3218.

25 V. Mckee, M. R. J. Dorrity, J. F. Malone, D. Marrs, J. Nelson, J. Chem. Soc. Chem. Commun., 1992, 383–386.

26 R. Menif, J. Reibenspies, A. E. Martell, *Inorg. Chem.*, 1991, **30**, 3446–3454.

27 M. G. Basallote, J. Duran, J. F. Trujillo, M. A. Manes, *J. Chem. Soc. Dalton Trans.*, 1999, 3817-3823.

28 M. G. Basallote, E. Blanco, M. Blazquez, M. J. F. Trujillo, R. Litran, M. A. Manez, M. R. D. Solar, *Chem. Mater.*, 2003, **15**, 2025–2032.

29 M. G. Basallote, E. Blanco, M. J. F. Trujillo, M. A. Manez, M. R. D. Solar, *Chem. Mater.*, 2002, **14**, 670–676.

30 S. O. Kang, D. Vandervelde, D. Powell, K. B. James, *J. Am. Chem. Soc.*, 2004, **126**, 12272–12273.

31 G. E. Alliger, M. Peter, C. C. Cummins, D. G. Nocera, *Inorg. Chem.*, 2010, **49**, 3697–3699.

32 P. S. Lakshminarayanan, E. Suresh, P. Ghosh, J. Am. Chem. Soc., 2005, **127**, 13132–13133.

33 L. Fabbrizzi, I. Faravelli, G. Francese, M. Licchelli, A. Perotti, A. Taglietti, *Chem. Commun.*, 1998, 971-972.

34 Y. Li, L. Jiang, X. Feng, T. Lu, *Cryst. Growth Des.*, 2008, **8**, 3689-3694.

35 Q. Lu, J. M. Latour, C. J. Harding, N. Martin, D. J. Marrs, V. McKee, J. Nelson, *J. Chem. Soc. Dalton Trans*., 1994, 1471-1478.

36 A. Desai, P. Mathur, A novel class of supramolecular compounds: compound of formula (IA) and (IB). Indian Patent. 369055, 2021. https://patentscope.wipo.int/search/en/detail.jsf?ocId=IN335044831&_cid=P12-L40W51-74422-2.

37 S. A. Sabra, S. A. Sheweita, M. Haroun, D. Ragab, M. A. Eldemellawy, Y. Xia, D. Goodale, A. L. Allan, A. O. Elzoghby, S. Rohani, *J. Pharm. Sci.*, 2019, **108**, 1713–1725.

38 Y. C. Chen, Q. Ye, T. Gong, J. Kunag, S. Li, *J. Pharm. Biomed. Sci.*, 2018, **8**, 79-83.

39 P. Mathur, M. Mori, H. Vyas, K. Mor, J. Jagtap, S. Vadher, K. Vyas, R. Devkar and A. Desai, *ACS Omega*, 2022, **7**, 45545–45555.

40 A. Desai, P. Mathur, Novel bis (hydroxy benzylidene) cyclic ketone based tetra-aza corand. Indian patent. 369745, 2021. https://patentscope.wipo.int/search/en/detail.jsf?docId=IN335044831&_cid=P10-KZQKS6- 63174-1.

41 R. Samineni, J. Chimakurthy, S. Konidala, Turk. *J. Pharm. Sci.*, 2022, **19**, 706–713.

42 P. A. Sutton, V. Cody G. D. Smith, J. Am. Chem. Soc., 1986, **108**, 4155–4158.

43 N. E. Aydin, *Int. J. Polym. Sci.*, 2020, **2020**, 1-13.

44 W. M. Samy, *Int. J. Drug Dev. Res.*, 2012, **4**, 195-204.

45 M. Shahnoor, K. Shadab, G. DM, B. KS, *J. Drug Deliv. Ther.*, 2017, **7**, 1-12.

46 M. Rahimi, R. Karimian, E. B. Noruzi, K. Ganbarov, M. Zarei, F. S. Kamounah, B. Yousefi, M. Bastami, M. Yousefi, H. S. Kafil, *Int. J. Nanomed.*, 2019, **14**, 2619-2636.